Global ^{137}Cs fallout inventories of forest soil across Japan and their consequences half a century later

Eriko Ito [a],[*], Satoru Miura [b], Michio Aoyama [c], Koji Shichi [d]

[a] Hokkaido Research Center, Forestry and Forest Products Research Institute, Hitsujigaoka 7, Toyohira-ku, Sapporo, 062-8516, Japan
[b] Forestry and Forest Products Research Institute, Matsunosato 1, Tsukuba 305-8687, Japan
[c] Faculty of Life and Environmental Sciences, Center for Research in Isotopes and Environmental Dynamics, Univ. of Tsukuba, Tennodai 1-1-1, Tsukuba, 305-8577, Japan
[d] Shikoku Research Center, Forestry and Forest Products Research Institute, 2-915 Asakuranishi, Kochi, 780-8077, Japan

A B S T R A C T

Japanese forests were exposed to multiple sources of radioactive contamination. To acquire scientific guidance on forest management planning, it is crucial to understand the long-term radiocesium (^{137}Cs) distribution (and redistribution) over time. To obtain robust evidence of the residual global fallout of ^{137}Cs (^{137}Cs-GFO) after a few decades, we determined ^{137}Cs-GFO inventory in forest soil at 1171 soil pits of 316 plots evenly spaced across Japan from 2006 to 2011, shortly before the Fukushima Dai-ichi Nuclear Power Plant accident. The activity concentration measurements were performed using a NaI well-type scintillation counter. The average ($\pm$SD) ^{137}Cs-GFO in forest soil (0–30 cm from the surface) of the National Forest Soil Carbon Inventory (NFSCI) sampling plots uniformly extracted from the entire country was estimated to be 2.27 $\pm$ 1.73 kBq m^{-2} ($n = 316$) as of Oct. 1, 2008. A high nationwide spatial variation was found in ^{137}Cs-GFO, where relatively high ^{137}Cs-GFO was found along the Sea of Japan compared with the total annual precipitation. We also obtained a reconstructed decay-corrected cumulative ^{137}Cs-GFO dataset from the fallout observatories as the initial ^{137}Cs-GFO. The cumulative ^{137}Cs-GFO of fallout observatories averaged 2.47 $\pm$ 0.95 kBq m^{-2} ($n = 39$) as of Oct. 1, 2008 and displayed spatial variation similar to that in forest soil. To identify whether ^{137}Cs-GFO remains in forest soil across Japan, we examined a general linear mixed-effect model comparing ^{137}Cs-GFO between forest soil and the observatory under normalized annual precipitation and region. The model did not indicate a significant difference, but relatively lesser ^{137}Cs-GFO was found in forest soil, where the least-squares mean of ^{137}Cs-GFO in forest soils was 79.1% of that of the observatory. The variation in ^{137}Cs-GFO in forest soils within NFSCI sampling plots was 1.4 times greater than that among plots. The high spatial variation in ^{137}Cs-GFO within a 0.1-ha plot strongly suggested the redistribution of ^{137}Cs-GFO within the forest catchment. The vertical distribution pattern of ^{137}Cs-GFO across three depth layers indicated that the ^{137}Cs-GFO redistributions were likely attributed to the movements of sediments and mass. Moreover, when extracting soil pits assumed to have the least soil disturbance from the vertical distribution pattern, no significant difference in ^{137}Cs-GFO was observed between forest soil and observatory data. These findings provide important insights into the stability of ^{137}Cs-GFO in the forest ecosystem. Considering the potential hotspot where ^{137}Cs-GFO can accumulate deeper in the soil (>30 cm in depth), most ^{137}Cs-GFO has remained in the forest for decades. Our study offers microscale heterogeneous ^{137}Cs-GFO distribution in forests for ensuring long-term forest management planning necessary for both the long-term migration and local accumulation of ^{137}Cs in forests.

1. Introduction

Radioactive emissions generated from the Fukushima Dai-ichi Nuclear Power Plant (FDNPP) accident have caused cesium-137 (^{137}Cs) fallout in forested areas (Hashimoto et al., 2012; Evrard et al., 2015; Nakajima et al., 2017). The consequence of the ^{137}Cs fallout in forested

areas is a major concern for local inhabitants. In particular, Japan is prone to sediment-related disasters (e.g., mass movements and soil erosion) caused by a combination of various geographical factors (e.g., rainfall, snowmelt, earthquake, soil, geological structure, and topography) (Yoshimatsu and Abe, 2006). Such disasters may result in a specific redistribution pattern of ^{137}Cs (Fukuyama et al., 2005). Japanese forests were exposed to global fallout of ^{137}Cs (^{137}Cs-GFO) produced from the nuclear weapon tests in the 1950s and 1960s. The investigation of the distribution of ^{137}Cs-GFO in forest soils after a few decades would provide useful insights into the future distribution of the FDNPP-generated ^{137}Cs fallout.

Many studies on the redistribution of ^{137}Cs fallout, both ^{137}Cs-GFO (Jagercikova et al., 2015) and ^{137}Cs fallout generated from the Chernobyl nuclear power plant in 1986 (Rafferty et al., 2000; Zhiyanski et al., 2008), have revealed the long-term persistence of ^{137}Cs in soil upon its adsorption onto clays (Dyer et al., 2000). Accordingly, the infiltration rate of ^{137}Cs in soils is the key factor in determining the vertical distribution of deposited ^{137}Cs on terrestrial ecosystems (Bunzl et al., 2000; Kirchner et al., 2009; Jagercikova et al., 2015). Numerous vertical migration studies have been a central part of the research determining the redistribution of ^{137}Cs (e.g., Bunzl et al., 1992; Zygmunt et al., 1998; Barišić et al., 1999; Rosén et al., 1999; Arapis and Karandinos, 2004; Shand et al., 2013).

A forest soil survey was conducted under the National Forest Soil Carbon Inventory (NFSCI) project from July 2006 to February 2011, shortly before the FDNPP accident (Ugawa et al., 2012; Nanko et al., 2017). In the NFSCI project, the forest surface soil, stratified into three layers (0–5, 5–15, and 15–30 cm in depth), was collected at systematically selected grid points over the forest sector. The NFSCI soil samples enabled us to determine the range and spatial distribution of the ^{137}Cs-GFO inventory in forest soils before the FDNPP accident throughout Japan; in other words, the baseline data for ^{137}Cs-GFO in forest ecosystems were obtained to investigate the dynamics of radioactive materials produced from the FDNPP accident. Moreover, the three-stratified soil-sampling design allowed us to investigate the vertical distribution of ^{137}Cs-GFO in soil profiles.

A well-established solution to assess the redistribution of ^{137}Cs fallout involves the use of the ^{137}Cs inventory in soils at reference sites, i. e., undisturbed sites unaffected by soil erosion and accretion (Walling and Quine, 1990; Wallbrink et al., 1994; Owens and Walling, 1996; Aoyama et al., 2006). Two nationwide assessments have also adopted the reference site approach to estimate the ground depositions of ^{137}Cs in the topsoil in Japan (Yamagata et al., 1966; Komamura et al., 1999). A possible technique of adapting this reference site approach for the aforementioned NFSCI soil samples involves classifying sampling points into reference sites and non-reference sites. The key limitation is whether the quality and quantity of the reference sites extracted from the NFSCI dataset are adequate for the ^{137}Cs redistribution analysis. Compared with the case in previous studies where the most appropriate point for a reference site is carefully selected within the catchment (Owens and Walling, 1996), it may be difficult to assure the same standard of the reference site for the NFSCI soil samples collected at systematically selected locations.

Another possible approach to evaluate the ^{137}Cs redistribution is the appropriate assessment of the decay-corrected cumulative deposition of ^{137}Cs-GFO (Parsons and Foster, 2011; Mabit et al., 2013). ^{137}Cs-GFO depositions have been measured using water-bed deposit systems at many stations across Japan (e.g., Katsuragi, 1983; Katsuragi and Aoyama, 1986). These fallout studies, as well as the nationwide assessments on the ^{137}Cs inventory in the topsoil as mentioned above (Yamagata et al., 1966; Komamura et al., 1999), strongly indicate the remarkably high spatial variation in the amount of cumulative ^{137}Cs-GFO, which significantly accumulated in the northwestern region along the Sea of Japan. After appropriately assessing the spatial variation of the cumulative ^{137}Cs-GFO, the comparison of the present ^{137}Cs-GFO inventory with the decay-corrected cumulative deposition of

^{137}Cs-GFO would provide insights into the redistribution of ^{137}Cs-GFO in the last few decades.

The primary aim of this study is to explore the consequences of ^{137}Cs-GFO in forested areas across Japan after half a century from fallout deposition. In particular, we (1) determine the amount of residual ^{137}Cs-GFO in forest soils using the soil sample archives for 316 evenly spaced plots, collected shortly before the FDNPP accident, (2) provide reconstructed decay-corrected cumulative depositions of ^{137}Cs-GFO for 39 observatories, (3) clarify the differences between the residual ^{137}Cs-GFO in forest soils and the cumulative ^{137}Cs-GFO obtained at observatories, and (4) assess the vertical distribution pattern of ^{137}Cs-GFO in the three soil layers to examine the secondary migration process of ^{137}Cs-GFO on slopes.

2. Materials and methods

2.1. Residual ^{137}Cs-GFO inventory in forest soils

2.1.1. Sampling design

We used soil samples collected during the NFSCI project from July 2006 to February 2011 (Ugawa et al., 2012; Nanko et al., 2017). Grid points (4 × 4 km) across the forest areas of Japan were systematically selected for the Forest Resources Monitoring Survey, in which tree censuses were conducted during FY 1999–2003 (Forestry Agency of Japan, 2012). One-fifth of these survey sites were selected for the NFSCI project. Of the 2404 plots of NFSCI, we examined the ^{137}Cs-GFO in 316 evenly spaced plots. The forest site properties, such as the soil group, forest type, microtopography, and slope inclination at soil pit, acquired during the survey are available at https://www.rinya.maff.go.jp/j/keika ku/tayouseichousa/chousadeta.html. The classification of soil groups is provided elsewhere (Forest soils division, 1975).

In NFSCI, soil samples from four soil pits were examined within a 1000-m^2 circular area of diameter of 35.68 m per plot (Supplementary Fig. 1, Ugawa et al., 2012). Four repetitions of the soil pit surveys were performed at a distance of 2.8 m from the north, east, south, and west (Supplementary Fig. 1, Ugawa et al., 2012). In each soil pit, soil samples were collected across three depth layers: 0–5, 5–15, and 15–30 cm. The bulk density and chemical properties (total carbon and nitrogen contents) of these samples were measured. A total of 1171 soil pits were obtained from 316 plots. Among the 316 plots, 251 plots were subjected to four repetitions of the soil pit surveys, while the other plots ($n = 65$) lacked soil pit repetitions owing to the overlapping of the pit location with a large rock, forest road, or water body. Among the 1171 soil pits, 1136 pits (97%) had complete soil collections of the three depth layers, while 26 and 9 pits lacked soil layers of depths 15–30 and 5–30 cm, respectively, mainly because of the presence of large rocks.

2.1.2. Measurement of the activity concentration of ^{137}Cs

The gamma rays of ^{137}Cs in each sample filled in a 20-mL vial were quantified using a NaI well-type scintillation counter (2480 WIZARD2 Automatic Gamma Counter, PerkinElmer, Inc., Waltham, MA, USA) for 1800 s. The ^{137}Cs gamma ray peak of 662 keV was treated using Code Fukushima software (Niki Glass Company Ltd., Tokyo, Japan; Yamada and Takano, 2014), and the net counts of the ^{137}Cs peak area were obtained using a maximum likelihood estimation. The NaI well-type scintillation counters were calibrated using certified multiple gamma-emitting large volume sources manufactured by the Japan Radioisotope Association and certificated by the Japan Calibration Service System to ensure traceability of radioactivity measurements. Four certified reference materials were also measured to make sure the comparability of the measurement using our system (Supplementary Table 1). We confirmed that the measurements are well within the range of uncertainties, except for the IAEA-444 reference material. The measurement results of IAEA-444 were 14%–24% higher than the certified value, possibly because of the fluctuations in peak identification using Code Fukushima software caused by the co-located ^{214}Bi peak.

This NaI gamma counter system can perform measurements with an expanded uncertainty of 6.6% for certified materials. We measured the unknown samples for 1800 s. This short measurement time resulted in relatively high measurement uncertainties. The expanded uncertainty combined with the measurement reproducibility obtained from four repeated measurements was 25.7% for the GFO soil samples. The mean expanded uncertainties for the GFO soil samples with activity concentrations of >100 Bq kg^{-1} were 26.4% and those for samples with concentrations of 50–100, 25–50, and <25 Bq kg^{-1} were 40.2%, 58.4%, and 54.7%, respectively. We also compared the NaI gamma counter measurements for 60 unknown samples with those obtained using high-purity Ge detectors (GEM20-70, GEM40P4-76, GEM-FX7025P4-ST, or GWL- 120-15-LB-AWT, ORTEC, Oak Ridge, US). The NaI gamma counter measurement results were consistent with the Ge detector measurement results within the measurement uncertainties (Supplementary Fig. 2).

The detection limit (DL) was set to twice a sigma of counting error. The quantified values of the samples below the DL were obtained by DL/ (square root 2) to conduct statistical analysis using all analyzed samples, including those with considerably low activity concentrations.

The ^{137}Cs-GFO inventory was calculated by multiplying the ^{137}Cs activity concentration, which was decay-corrected to October 1, 2008 (i. e., the intermediate point in the soil-sampling period) data using a half-life of 30.2 years for ^{137}Cs, a layer thickness of 30 cm, and the bulk density of the soil sample. The ^{137}Cs-GFO activity concentration in terms of Bq kg^{-1} for the forest surface soil (0–30 cm in depth) was obtained by dividing the total amount of ^{137}Cs-GFO activity by the soil mass. Hereafter, we refer to this dataset as "Forest Inventory" data, which were provided on a soil pit basis and plot basis (i.e., the average of the soil pit replication within a single plot). The latter data were partially reported by Miura et al. (2015a)).

2.1.3. Vertical distribution pattern of ^{137}Cs-GFO in forest soils

To determine whether the ^{137}Cs-GFO redistribution has occurred in decades, we quantified the vertical distribution of ^{137}Cs-GFO in the three soil layers for soil pits with complete three depth layers ($n = 1136$). To assess the relative accumulation of ^{137}Cs-GFO in each soil layer, we introduced two indices: the percentage of ^{137}Cs-GFO amount for each soil layer to the total of soil pit (P_n, %) for each nth soil layer, where n represents the order of the soil layer (1, 0–5 cm; 2, 5–15 cm; and 3, 15–30 cm in depth), and the amount of ^{137}Cs-GFO per unit depth for each soil layer (Q_n, kBq m^{-2} cm^{-1}). According to our pre-analysis, the frequency distribution of P_n showed a highly concave shape (data not shown); that is, several soil pits had very little ^{137}Cs-GFO in any layer ($P_n \approx 0$) or had a layer in which almost all ^{137}Cs-GFO concentrated ($P_n \approx$ 100). We set the threshold to $P_n < 0.5\%$ for a layer having "little" ^{137}Cs-GFO accumulation. We expect the upper soil layer in undisturbed sites to exhibit high P_n values; otherwise (i.e., $P_n < 0.5\%$ for upper soil layers), it can be inferred that considerable subsoil could migrate and redeposit in the wake of large-scale soil disturbance. Another index we focused on was the magnitude relation of Q_n within a single soil pit, which is an important feature in characterizing the vertical distribution. Owing to the long-term presence of ^{137}Cs in the soil under high ^{137}Cs absorption onto clays (Dyer et al., 2000) and slow downward migration rates within mineral soils (Zygmunt et al., 1998), we expect the upper soil layer to show higher Q_n; otherwise, it can be inferred that there was some disturbance. We categorized the vertical distribution pattern using the two indices on the three layers of each soil pit. The mean $\pm$ SD of the field-measured slope for each vertical distribution pattern was calculated. We assessed the relation between the inventory of ^{137}Cs-GFO and the categorized vertical distribution pattern (Section 2.6.4), based on which we evaluated the possibilities of erosion and downward migration loss of ^{137}Cs-GFO.

2.2. Decay-corrected cumulative ^{137}Cs-GFO activity at meteorological observatories

The ^{137}Cs-GFO depositions have been observed at many stations across Japan. The observations began as early as the late 1950s, with the largest number of stations conducting observations in the late 1960s (IGFD database, Aoyama, 2019; Environmental Radiation Database, the Secretariat of the Nuclear Regulation Authority, https://search. kankyo-hoshano.go.jp/servlet/search.top). However, the cumulative deposition of ^{137}Cs-GFO from the beginning of nuclear testing was available only at a few observatories. Most stations in the district and local meteorological observatories and local authorities lack data on the earliest and largest depositions in the spring of 1963. To encompass the nationwide variation in the cumulative deposition of ^{137}Cs-GFO, we collected monthly data on the deposition of ^{137}Cs-GFO from as many observatories as possible, and thus reconstructed the decay-corrective cumulative ^{137}Cs-GFO until December 2005 through temporal interpolation between the observatories.

The Japan Meteorological Agency (JMA) has been observing both long- and short-term ^{137}Cs fallout (Supplementary Table 2, Supplementary Fig. 3a). The earliest ^{137}Cs data were collected by the Meteorological Research Institute (MRI) at Tokyo in April 1957. Then, in July 1959, ^{137}Cs observations were performed in five regional headquarters (Sapporo, Sendai, Tokyo, Osaka, and Fukuoka) of JMA and one local meteorological office (Akita) (Supplementary Table 2).

The decay-corrected cumulative depositions of ^{137}Cs-GFO as of October 1, 2008, was first estimated by the earliest observation observatory, JMA (Tokyo). The lack of ^{137}Cs data for July 1945 to March 1957 was interpolated by the reconstructed values from the total amount of atmospheric nuclear explosion for the Kanto Plain (17000 km^2), including Tokyo (Aoyama, 1999). No data were available on MRI (Tokyo) after April 1980, due to the relocation of the institute to Tsukuba, located 60 km northeast of MRI (Tokyo). For April 1980 to December 2005, measurements of the Tokyo Meteorological Observatory, located 10 km southeast east of MRI (Tokyo), were substituted.

Second, the decay-corrected cumulative depositions of ^{137}Cs-GFO were estimated for the second earliest six observatories, where data were available from July 1959. Data on ^{137}Cs-GFO from July 1945 to June 1959 for the six observatories were estimated by MRI (Tokyo). We calculated the ratios of ^{137}Cs deposition from July 1959 to March 1980 between each observatory and MRI (Tokyo). The estimated values from July 1945 to June 1959 were obtained by multiplying the cumulative value during this period obtained from MRI (Tokyo) with the ratio of the values obtained from any observatory and MRI (Tokyo) studies, assuming that the ratios were constant throughout the period because the fallout should be global. The ratios of the total precipitation at each observatory from July 1959 to March 1980 to the total precipitation in Tokyo during the same period were calculated (Supplementary Table 2). We also calculated the ratio of the total annual precipitation for each year from 1945 to 2005 at each observatory to the annual precipitation for each year in Tokyo and obtained the average $\pm$ SD of the ratio (Supplementary Table 2). The ratio of the total precipitation from July 1959 to March 1980 is within the range of the average $\pm$ SD of the total annual precipitation ratio for each year, indicating that the estimation errors caused by rainfall outliers during the measurement period are considerably suppressed (Supplementary Table 2).

Monitoring of ^{137}Cs-GFO deposition has been also performed in some local meteorological observatories ($n = 8$, including MRI-Tsukuba) and local authority offices of prefectural institutes of public health ($n = 24$); however, these were performed for relatively short periods (2–7 years, Supplementary Tables 2 and 3, Supplementary Figs. 3a and 3b). Although these short-term measurements began in the late 1960s or later and the largest depositions during the early 1960s were not included from these measurements, the decay-corrected cumulative depositions of ^{137}Cs-GFO were also estimated by these observatories. Choosing the data for a certain period overlapping between the target

observatory and the seven observatories mentioned in the previous paragraph, we estimated ^{137}Cs-GFO of the local observatories. This method provided seven estimates, in which the average and SD values of ^{137}Cs-GFO were obtained. The monthly ^{137}Cs fallout was recorded to the nearest 2 decimal places in mC_i km^{-2}. Hereafter, we refer to this dataset as "Observatory" data. Similar to the six observatories mentioned in the previous paragraph, the ratios of the total precipitation between Tokyo and other individual stations were within the range of the average $\pm$ SD of the total annual precipitation ratio for each year from 1945 to 2005, suggesting that the ratios of the total precipitation were considerably constant throughout the measurement period (Supplementary Tables 2 and 3).

Note that the data reliability for the samples collected by the local authority was questionable because these samples were analyzed by the Japan Analytical Chemistry Research Institute. The laboratory was revoked in 1974 for reasons of data fabrication. Our explorative analyses indicated that the amount of monthly ^{137}Cs-GFO depositions collected by local authority offices were relatively small compared with that collected by the observatories of JMA within the same city and month (Supplementary Fig. 4).

2.3. Ground deposition of ^{137}Cs in soil and global ^{137}Cs-GFO estimation reported in previous studies

For comparison with the Forest Inventory data, we utilized two studies by Yamagata et al. (1966) and Komamura et al. (1999) on the ground deposition of ^{137}Cs in topsoil across Japan. Yamagata et al. (1966) examined the ground deposition of ^{137}Cs in undisturbed soil at open and flat sites up to a depth of 5 cm in August 1965. They set the following conditions for sampling plot selection: non-subjected to soil transfer and cultivation over the past 10 years; non-covered with trees, i. e., with a clear view of the sky; the soil surface has little vegetation, except for small plants such as moss, and flat area. They, therefore, chose the grounds of the shrines and temples, the schoolyard of an elementary school, and the yard of an old farmhouse, where they confirmed the lack of soil transfer and cultivation. They collected soil samples from 212 sampling plots, in which they rejected ^{137}Cs data from 40 plots, without stating any reason. They divided the soil-sampling plots into 22 regions based on the climate characteristics and reported regional average values only ($n = 172$). The number of sampling plots for each region is shown in Supplementary Table 4. Komamura et al. (1999) reported the ground deposition of ^{137}Cs in paddy topsoil for a depth of 10–15 cm in January 1964 from 14 sampling plots. The data in Yamagata et al. (1966) and Komamura et al. (1999) were recorded as an integer in mC_i km^{-2} and up to 2 decimal places in kBq m^{-2}, respectively. The ground deposition of ^{137}Cs previously reported in Yamagata et al. (1966) and Komamura et al. (1999) did not include fallout after the collection of soil samples. Therefore, we estimated that the provided values were as of October 1, 2008, in kBq m^{-2}. To normalize the cumulative period of the ground deposition of ^{137}Cs, we estimated the ratio of deposition from July 1945 to July 1965 or July 1945 to December 1963 to the total deposition from July 1945 to December 2005, based on the MRI (Tokyo) data. The ratios were estimated to be 0.802 and 0.682 for July 1945–July 1965 and July 1945–December 1963, respectively. Using these values as correction factors, the amounts of ground deposition of ^{137}Cs until December 2005 were estimated for these two previous studies. Hereafter, we refer to these datasets as "Yamagata" data and "Komamura" data.

To confirm the range of our estimated initial ^{137}Cs-GFO, we referenced studies on global reconstruction of the spatial distribution of ^{137}Cs-GFO using global measurements of ^{137}Cs-GFO in rain, seawater, and soil, with a grid resolution of $10° \times 10°$ (Aoyama et al., 2006). Aoyama et al. (2006) provided the range of ^{137}Cs-GFO over Japan as 4.16–10.63 kBq m^{-2} as of January 1, 1970. For comparison, we converted this range to that of October 1, 2008. We refer to the estimated range of ^{137}Cs-GFO as Aoyama data. The ratio of the deposition for July

1945–December 1969 to the total deposition for July 1945–December 2005 based on the MRI (Tokyo) data was estimated to be 0.879.

2.4. Total annual precipitation

The total annual precipitation at the JMA observatories was obtained from the JMA website (http://www.data.jma.go.jp/gmd/risk/obsdl/index.php). The total annual precipitation for local authority offices was substituted with the nearest JMA weather station data. Precipitation data for NFSCI plots were obtained from the normal value of the total monthly precipitation map, with 1 km resolution, based on the meteorological dataset from 1981 to 2010 (Japan Meteorological Agency, 2012). The total annual precipitation data were obtained for sampling plots in Yamagata et al. (1966) and Komamura et al. (1999), as well as the NFSCI plots. In Yamagata et al. (1966), the locations of soil-sampling plots were specified at the municipal level. We examined the regional average of the total annual precipitation for Yamagata's soil-sampling plots.

2.5. Classification of soil-sampling plots and soil pits (region, soil group, forest type, and sediment movement categories)

We divided the NFSCI soil-sampling plots into 23 regions based on the climate characteristics (Supplementary Fig. 3c). The regional classification conforms to Yamagata et al. (1966). We added one region category, including Okinawa Prefecture, Amami islands, and ocean islands located in the South of Japan, which were not included in Yamagata et al. (1966), because of the American occupation of Okinawa. We also divided the Observatory data and Komamura data into 23 regions, each divided into two groups: the area along the Sea of Japan (Regions of 2, 4, 6, 13, 16, and 20, Supplementary Fig. 3c) and the rest. Hereafter, we refer to the former as the Sea of Japan side and the latter as the Pacific Ocean side, for convenience.

We divided the 316 NFSCI soil-sampling plots into nine soil groups and five forest types based on the plot basis data (Supplementary Tables 5 and 6, and see Section 2.1.1 for the data source).

We classified the 1171 soil pits into three sediment movement categories, i.e., erosion, accumulation, and reference, based on microtopography and slope inclination of the soil pit basis data (Supplementary Table 7). The determination that the soil pit classified as a reference in the sediment movement category, i.e., it is flat and unaffected by sediment transport, was based on a slope of 5° or less. This is based on reports that landslides in Japan occur on gentle to moderate slopes of 5–30° (The Japan Society of Landslide and National Conference of Landslide Control, 2002). The reference sites ($n = 111$) included top plateau for flat areas on the slope top ($n = 71$) and flatland for flat areas unrelated to the slope ($n = 40$). Other soil pits were classified into erosion or accumulation based on slope position and curvature, where the location with upper or convex slope was classified as erosion ($n = 903$) and the location with lower or concave slope was classified as accumulation ($n = 157$).

2.6. Model analysis

2.6.1. Relations between the ^{137}Cs-GFO inventory and total annual precipitation

Generally, a good relationship between the ^{137}Cs-GFO and annual precipitation amount can be expected globally (Aoyama et al., 2006). We examined the relations between ^{137}Cs-GFO and annual precipitation for each dataset category (Forest Inventory on a plot basis, Observatory, Yamagata, and Komamura datasets). We tested whether the relationship was different between the area groups (i.e., Sea of Japan side and Pacific Ocean side), by using a general linear model to estimate ^{137}Cs-GFO using factors such as the total annual precipitation, area group, and the interaction of total annual precipitation and area group as fixed effects.

2.6.2. Difference in the ^{137}Cs-GFO inventory based on regions and forest site properties

We ascertained whether ^{137}Cs-GFO of the Forest Inventory was different among regions under normalized and non-normalized total annual precipitation. We used a general linear mixed-effect (GLM) model to estimate ^{137}Cs-GFO using region and total annual precipitation (when normalized precipitation) as fixed effects, and sampling plots for NFSCI as a random effect. Post hoc comparisons among regions were conducted using the Tukey-HSD test ($p < 0.05$).

Similarly, we tested whether the ^{137}Cs-GFO of the Forest Inventory varied depending on the site properties (soil group and forest type) under normalized and non-normalized total annual precipitations using GLM models similar to that used above.

2.6.3. Difference in the ^{137}Cs-GFO inventory among the dataset categories

We tested the hypothesis that there is no significant difference in ^{137}Cs-GFO inventory among the dataset categories. We examined this hypothesis within a frame of the GLM model, using total annual precipitation, regions, and dataset categories as fixed effects and sampling plots for NFSCI as a random effect. The most accurate predictive model was identified as that with the lowest Bayesian information criterion (Schwarz, 1978), where a fixed effect of the interaction of total annual precipitation and regions was rejected. Post hoc comparisons among dataset categories were examined using the Tukey-HSD test ($p < 0.05$).

For each subset of the Forest Inventory data divided by the sediment movement category, we tested the hypothesis that there is no significant difference in ^{137}Cs-GFO inventory among the dataset categories. We expected that (1) the ^{137}Cs-GFO of the Forest Inventory is significantly small when extracting the subset of erosion, (2) there is no significant difference when extracting the subset of reference, and (3) the ^{137}Cs-GFO of the Forest Inventory is significantly large when extracting the subset of accumulation. We conducted a similar analysis, i.e., the GLM model using the total annual precipitation, regions, and dataset categories as fixed effects and sampling plots for NFSCI as a random effect, for each subset of the Forest Inventory data divided by the sediment movement category. When the dataset category was found to be a significant explanatory variable, post hoc comparisons among dataset categories were conducted using the Tukey-HSD test ($p < 0.05$).

We tested the hypothesis that there is no significant difference in the ^{137}Cs-GFO inventory between the Forest Inventory and the Observatory for a subset of the Forest Inventory data divided by the vertical distribution pattern. We examined this hypothesis within a frame of the GLM model, using the total annual precipitation, regions, and dataset categories (Forest Inventory or Observatory) as fixed effects and the sampling plots for NFSCI as a random effect. Post hoc comparisons among dataset categories were examined using the Tukey-HSD test ($p < 0.05$).

2.6.4. Difference in ^{137}Cs-GFO inventory of the Forest Inventory within an NFSCI sampling plot

For the Forest Inventory data, four repetitions of the soil pit surveys within a sampling plot allowed us to compare the effects of the soil pit properties on the ^{137}Cs-GFO inventory under normalized conditions of differences in cumulative ^{137}Cs-GFO depositions at each sampling site. We examined what percentage of the variability in the ^{137}Cs-GFO inventory could be explained by the differences in the NFSCI sampling plots, within the frame of the GLM model using the ^{137}Cs-GFO inventory as an objective variable and the NFSCI sampling plots as a random effect term.

We tested the hypothesis that there is no significant difference in the inventory of ^{137}Cs-GFO of the Forest Inventory among soil pits differing in sediment movement category within an NFSCI sampling plot, within the frame of the GLM model using the sediment movement category as a fixed effect and the NFSCI sampling plots as a random effect.

We tested the hypothesis that there is no significant difference in the inventory of ^{137}Cs-GFO of the Forest Inventory among soil pits differing in vertical distribution pattern within an NFSCI sampling plot, using the vertical distribution pattern as a fixed effect and the NFSCI sampling plots as a random effect. Post hoc comparisons among vertical distribution patterns were examined using the Tukey-HSD test ($p < 0.05$).

We tested whether the slope was different for each vertical distribution pattern using ANOVA.

2.6.5. Vertical distribution patterns of neighboring soil pits

We analyzed whether soil pits within a plot (up to 4 pits in a plot) display an identical vertical distribution pattern. We computed the percentages of the vertical distribution patterns of neighboring soil pits for each vertical distribution pattern of a given soil pit for 3256 pairs of a given soil pit and its neighboring soil pit. We tested the null hypothesis that the vertical distribution pattern of neighboring soil pits (i.e., the other soil pits in the same plot for a given soil pit) is not significantly different from the vertical distribution pattern of a given soil pit. We used χ^2 contingency analysis to compare the observed vertical distribution pattern (for a given soil pit) with the expected vertical distribution pattern for the soil pit within the same NFSCI sampling plot. When the contingency analysis revealed statistical significance ($\alpha = 0.05$), we also computed χ^2 values for each cell. There are no post hoc comparisons for contingency analysis; thus, it cannot be determined if the deviation is statistically different from the expected value for each cell in the matrix. The computed χ^2 values for each cell were used to determine which cell was more or less compared to the expected value.

2.6.6. Simulation of the percentage of residual ^{137}Cs in the forest ecosystem

We simulated how the percentage of ^{137}Cs remained in the forest ecosystem given a fixed sediment runoff ^{137}Cs rate. If the amount of ^{137}Cs deposition in year t is X_t and the fixed sediment runoff ^{137}Cs rate is r, the residual amount (R_T) at year T can be expressed by the following equation: $R_T = X_t (1-r)^{(T-t)}$. If year T is 2005 and adding R_T for year t in the range from 1945 to 2005, we obtain the residual ^{137}Cs in the forest ecosystem in 2005. The percentage of residual ^{137}Cs in the forest ecosystem is calculated from the residual amount and the cumulative ^{137}Cs deposition. We used the chronological MRI measurements of ^{137}Cs-GFO (Tokyo) from July 1945 to March 1980 and MRI measurements (Tsukuba) from April 1980 to December 2005 for this simulation.

Statistical analysis was performed using JMP statistical software (Version 10.0, SAS Institute Inc.).

3. Results

3.1. Residual ^{137}Cs-GFO in forest soils (Forest Inventory data)

3.1.1. Overall status of residual ^{137}Cs-GFO in forest soils

The inventory of ^{137}Cs-GFO in forest soils (0–30 cm in depth) was estimated on a sampling plot basis. The average $\pm$ SD ($\pm$SE) of 316 sampling plots was 2.27 ± 1.73 ($\pm$0.10) kBq m^{-2} (ranging from 0.09 to 9.43 kBq m^{-2}, $n = 316$). A left-biased distribution peaking at ca. 1.5 kBq m^{-2} was found (Fig. 1a). A wider range and L-shaped frequent distribution were presented on a soil pit basis, and the average $\pm$ SD ($\pm$SE) of 1171 soil pits was 2.29 ± 2.30 ($\pm$0.07) kBq m^{-2} (ranging from 0.00 to 22.89 kBq m^{-2}, Fig. 1b). The geometric mean and median were 1.35 and 1.68 kBq m^{-2}, respectively.

The average ($\pm$SD) activity concentration of ^{137}Cs-GFO for forest soil (0–30 cm in depth) was 19.1 ± 25.8 Bq kg^{-1} (ranging from 0.0 to 355.2 Bq kg^{-1}) on a soil pit basis. The geometric mean and median were 10.0 and 11.8 Bq kg^{-1}, respectively. The topsoil layer (0–5 cm) showed the highest ^{137}Cs concentration in each soil pit profile in most cases ($n = 929$, 79% in total), while the highest ^{137}Cs concentration was sometimes found in the second layer (5–15 cm, $n = 178$, 15%) or the third layer (15–30 cm, $n = 64$, 6%). The former was found in almost all NFSCI plots ($n = 311$, 98% in total), whereas the latter was frequently found in NFSCI plots ($n = 164$, 52% in total).

Of the samples in each layer, the ^{137}Cs activity concentrations of 25% ($n = 297$) in the top layer, 60% ($n = 700$) in the second layer, and 90%
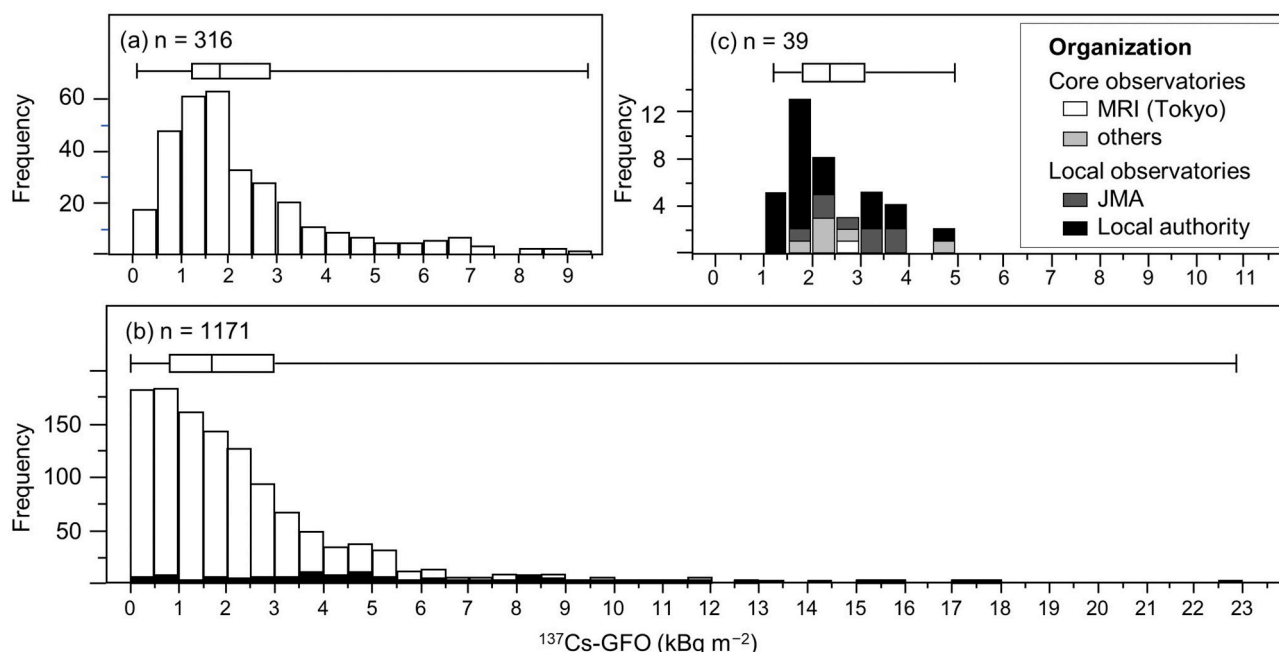
Fig. 1. Frequency distribution of ^{137}Cs-GFO in Japan (kBq m^{-2}). (a) Forest Inventory data on a plot basis, (b) Forest Inventory data on a soil pit basis, and (c) Observatory data. The box–whisker plots mark the minimum and maximum, and the 25th, 50th, and 75th percentile points. The value of ^{137}Cs-GFO is shown as of Oct. 1, 2008. Black columns in (b) indicate 66 soil pits that were above the detection limit in all three soil depth layers.

($n = 1019$) in the third layer were below the DL (Supplementary Fig. 5). The soil pits, where all the three layers were above the DL, were 6% ($n = 66$) of the whole. A high frequency of relatively large Q_n (the amount of ^{137}Cs-GFO per unit depth for each soil layer) values was clearly found in the first layer; the frequency distribution showed an extreme L-shape in the lower layer (Supplementary Fig. 5). However, considerable large Q_n values were scattered in the second and third layers as well, and these Q_n values were comparable to those of the first layer (ca. 0.3–1.5 kBq m^{-2} cm^{-1}, Supplementary Fig. 5).

3.1.2. Vertical distribution patterns of residual ^{137}Cs-GFO in forest soils

We divided the vertical distribution pattern of ^{137}Cs-GFO into nine types (Table 1). Type 6 (29.0% of total soil pits) was the most frequent pattern. In Type 6, ^{137}Cs-GFO accumulated mainly in the first layer and gradually decreased with depth. Type 4 was the second most frequent pattern (23.3%), where ^{137}Cs-GFO mainly accumulated in the first layer and somewhat existed in the second layer, but rarely in the third layer. These two types accounted for more than 50% of the total soil pits. Type 6 and Type 4 were found in 208 and 187 NFSCI plots, or 65.8% and 59.2% of the total NFSCI plots, respectively.

Several soil pits contained one or two layers with a low ^{137}Cs-GFO content ($\exists n : P_n < 0.5\%$, Types 1–5, 46.4% in total, Table 1). Type 2 (6.5%) had a distinctive feature in terms of ^{137}Cs-GFO accumulation only in the first layer. Contrary to Type 2, Type 1 was characterized by no accumulation in the first layer (4.3%). Type 1 was subdivided into three subtypes. Subtype 1a had accumulation in both the second and third layers. Subtypes of 1b and 1c were defined by no accumulation in the second and third layers, respectively. Type 3 (6.1%) was characterized by no accumulation in the second layer.

Type 5 (6.2%) and Type 7 (9.0%) were similar to Type 4 and Type 6, respectively. Both Type 5 and Type 7, however, showed a higher amount of ^{137}Cs-GFO per unit depth in the second layer than that in the first layer ($Q_1 < Q_2$). Type 8 was characterized by the lowest amount of ^{137}Cs-GFO per unit depth in the first layer than that in the other layers (5.7%). Note that Type 3 (6.1%) and Type 9 (9.6%) displayed little or lesser ^{137}Cs-GFO accumulation in the second layer compared to those in the first and third layers.

Types 6, 4, and 2 (58.9% of the total) were common in the gradually decreasing ^{137}Cs-GFO pattern throughout the three layers. The others (Types 1, 3, 5, 7–9 comprised 41.1% of the total) showed that ^{137}Cs-GFO-contaminated soil layers were covered by redeposition with fewer ^{137}Cs-GFO-contaminated soil materials. On average, ^{137}Cs-GFO mainly accumulated in the topsoil layer (51 ± 31% of total), followed by the second layer (34 ± 27%) and the third layer (16 ± 23%).

There was no significant difference in the slope inclination by the vertical distribution pattern ($p = 0.65$, Table 1, Model 2.6.4).

3.2. Cumulative ^{137}Cs-GFO at meteorological observatories (observatory data)

The average (±SD) cumulative ^{137}Cs-GFO for fallout observatories was 2.47 ± 0.95 kBq m^{-2} as of October 1, 2008 (n = 39), ranging from 1.23 to 5.00 kBq m^{-2} (Fig. 1c).

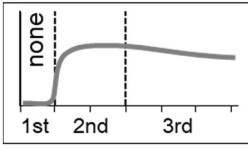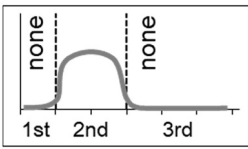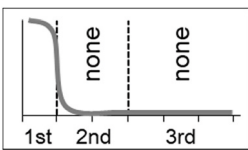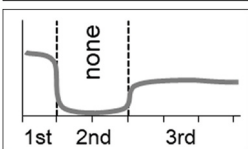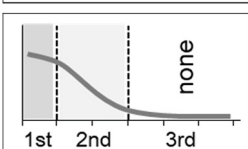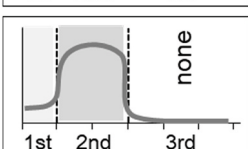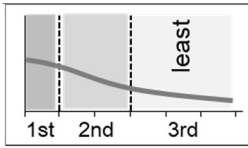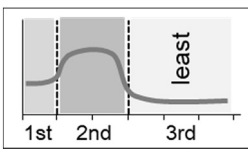The ^{137}Cs-GFO deposition in Tokyo was estimated to be 2.73 kBq m^{-2} as of October 1, 2008 (Table 2). The value was composed chiefly of the measurements conducted by MRI (Tokyo) from April 1957 to March 1980 (2.41 kBq m^{-2}, 88.1% of the total), the measurements conducted by the Tokyo Meteorological Observatory, located 10 km southeast east of MRI (Tokyo), from April 1980 to December 2005 (0.13 kBq m^{-2}, 4.9% of total), and the reconstructed value of the Kanto Plain from July 1945 to March 1957 (0.19 kBq m^{-2}, 7.0% of the total, Aoyama, 1999). The observatory measurements accounted for 93% of the estimated values, which was the highest percentage among the 39 observatories. The highest monthly deposition of ^{137}Cs-GFO was recorded by MRI (Tokyo) as 0.55 kBq m^{-2} month^{-1} in June 1963. The decay-corrected cumulative ^{137}Cs-GFO peaked for 1966–1969, and was estimated to be around 5.9–6.0 kBq m^{-2}.

The ^{137}Cs-GFO depositions at the other six long-term observatories were estimated to be around 2.5 kBq m^{-2} but ranged from 1.85 (Osaka) to 5.00 (Akita) kBq m^{-2} (Table 2). The values were composed chiefly of measurements at each observatory from July 1959 to December 2005 (ca. 75% of total) and of the reconstructed value from July 1945 to June 1959 from MRI (Tokyo) data (ca. 25% of total).

The ^{137}Cs-GFO estimates for JMA short-term observatories

Table 1
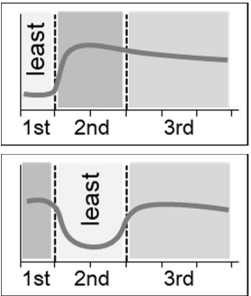Pattern classification of the vertical distribution of ^{137}Cs-GFO within a soil pit with a schematic diagram showing the relative magnitude of ^{137}Cs-GFO accumulation in the three layers. The assumed surface soil movement processes and the results of comparison between subsets of the Forest Inventory by types and the Observatory data, as well as the least-squares mean with statistical significance, are also described.

Type (Subtype)	Condition*$n = \{1, 2, 3\}$	Schematic diagram of Type[†]	No. (%) of soil pits	No. (%) of sites appeared	Assumed secondary migration processes of soil	Least-squares mean of ^{137}Cs-GFO (kBq m^{-2}) Forest inventory[‡]	Observatory	Slope inclination Mean ± SD (°)
	$\exists n : Pn < 0.5$							
1	$P_1 < 0.5$		49 (4.3%)	47 (14.9%)		1.67[n.s.]	2.15	26 ± 14
(1a)	$P_1 < 0.5 \wedge P_2 \geq 0.5 \wedge P_3 \geq 0.5$		27 (2.4%)	25 (7.9%)	Subsoil redeposition	1.97[n.s.]	2.19	26 ± 14
(1b)	$P_1 < 0.5 \wedge P_2 < 0.5 \wedge P_3 \geq 0.5$		10 (0.9%)	10 (3.2%)	High subsoil redeposition, Landslides	1.26[n.s.]	2.10	27 ± 17
(1c)	$P_1 < 0.5 \wedge P_2 \geq 0.5 \wedge P_3 < 0.5$		12 (1.1%)	12 (3.8%)	Erosion (or creep) and subsoil redeposition	0.61*	2.41	26 ± 14
2	$P_1 \geq 0.5 \wedge P_2 < 0.5 \wedge P_3 < 0.5$		74 (6.5%)	61 (19.3%)	Fast erosion	0.77*	2.37	27 ± 13
3	$P_1 \geq 0.5 \wedge P_2 < 0.5 \wedge P_3 \geq 0.5$		69 (6.1%)	63 (19.9%)	Multiple redeposition (first subsoil, then topsoil), Landslides	0.94*	2.38	23 ± 13
4	$P_1 \geq 0.5 \wedge P_2 \geq 0.5 \wedge P_3 < 0.5 \wedge Q_1 \geq Q_2$		265 (23.3%)	187 (59.2%)	Slow erosion or creep	1.71*	2.55	26 ± 13
5	$P_1 \geq 0.5 \wedge P_2 \geq 0.5 \wedge P_3 < 0.5 \wedge Q_1 < Q_2$		70 (6.2%)	65 (20.6%)	Multiple erosion (or creep) and redeposition	1.79[n.s.]	2.41	24 ± 14
	$\forall n : 0.5 < P_n$							
6	$Q_3 \leq Q_2 \leq Q_1$		330 (29.0%)	208 (65.8%)	Stable	2.35[n.s.]	2.53	25 ± 13
7	$Q_3 \leq Q_1 < Q_2$		102 (9.0%)	87 (27.5%)	Continuous redeposition	2.95[n.s.]	2.25	24 ± 12
8	$Q_1 < Q_2 \wedge Q_1 < Q_3$		65 (5.7%)	58 (18.4%)	High continuous	3.66[n.s.]	2.73	26 ± 16

(continued on next page)

Table 1 (*continued*)

Type (Subtype)	Condition* $n = \{1,2,3\}$	Schematic diagram of Type†	No. (%) of soil pits	No. (%) of sites appeared	Assumed secondary migration processes of soil	Least-squares mean of ^{137}Cs-GFO (kBq m^{-2})		Slope inclination Mean ± SD
					redeposition, Mixture of topsoil and subsoil	Forest inventory‡	Observatory	(°)
9	$Q_2 \leq Q_1 \wedge Q_2 < Q_3$		79 (6.8%)	69 (21.8%)	Multiple redeposition, Mixture of topsoil and subsoil	1.54*	2.51	27 ± 12
Total			1136	316				25 ± 13

*P_n is the percentage of ^{137}Cs-GFO for nth soil layer to the total of the soil pit (%); Q_n is the amount of ^{137}Cs-GFO per unit depth for the nth soil layer (kBq m^{-2} cm^{-1}). †Soil pits are shown sideways, where the left side represents the surface and three layers in the order of depth from the surface. Gray thick lines indicate the relative amount of ^{137}Cs-GFO in three layers based on P_n. The gray scale of the panel showing each layer indicates the magnitude relation of the ^{137}Cs-GFO amount per unit depth (Q_n), which is shown only for Types that include Q_n in the judgment conditions (Types 4–9). The darker panel indicates larger Q_n. ‡Asterisk (*) indicates a significant difference between the subsets of the Forest Inventory and the Observatory data ($p < 0.05$).

Table 2
Long-term decay-corrected cumulative depositions of ^{137}Cs-GFO at the observatories conducting long-term observations.

Collection period	MRI (kBq m^{-2})		Meteorological observatory (kBq m^{-2})						References
	Tsukuba	Tokyo	Sapporo	Akita	Sendai	Tokyo	Osaka	Fukuoka	
Jul. 1945–Dec. 1956		*0.17*	0.16	0.31	0.17	0.15	0.12	0.15	1)
Jan. 1957–Mar. 1957		*0.02*	0.02	0.04	0.02	0.02	0.01	0.02	1, 2, 3)
Apr. 1957–Dec. 1957		0.13	0.12	0.24	0.13	0.12	0.09	0.12	2, 3)
Jan. 1958–Dec. 1958		0.13	0.12	0.24	0.13	0.12	0.09	0.12	2, 3)
Jan. 1959–Jun. 1959		0.22	0.21	0.40	0.22	0.20	0.15	0.20	2, 3)
Jul. 1959–Aug. 1961		0.16	0.10	0.21	0.11	0.16	0.10	0.08	2, 3)
Sep. 1961–Dec. 1979		1.76	1.69	3.25	1.81	1.57	1.20	1.64	2, 3)
Jan. 1980–Mar. 1980		0.00	0.00	0.00	0.00	0.00	0.00	0.00	3, 4)
Apr. 1980–Dec. 1982	0.02	(0.02)	0.02	0.04	0.03	0.02	0.03	0.02	3, 4)
Jan. 1983–Dec. 2005	0.09	(0.11)	0.05	0.26	0.10	0.11	0.05	0.06	5)
Total	2.73		2.50	5.00	2.73	2.48	1.85	2.41	

Values are as of Oct. 1, 2008. The Italic numbers from Jul. 1945 to Mar. 1957 for MRI (Tokyo) are estimated values from atmospheric nuclear explosion total amounts. The numbers in parenthesis from Apr. 1980 to Dec. 2005 for MRI (Tokyo) are substitute values to fill the observation blank by data on Tokyo Meteorological Observatory. The underlined numbers from Jul. 1945 to Jun. 1959 for meteorological observatories are estimated values proportionally calculated from the data on MRI (Tokyo).References: 1) Aoyama, 1999; 2) Katsuragi, 1983; 3) Geochemical Research Department, 1996; 4) Katsuragi and Aoyama, 1986; 5) Japan Meteorological Agency, 2007. Data from 1945 to 1999 are available elsewhere (Aoyama and Hirose, 2002).

(Supplementary Table 2) and local authorities (Supplementary Table 3) are shown in Table 3. The percentages of the observed ^{137}Cs-GFO depositions to the total estimated ^{137}Cs-GFO depositions were relatively small (1.1–8.4% and 20.1% for JMA observatories and local authorities, respectively, Table 3).

3.3. Ground and global deposition of ^{137}Cs in previous studies (Yamagata, Komamura, and Aoyama data)

The regional averages of the ground deposition of ^{137}Cs in undisturbed soil (5 cm in depth) in August 1965, based on Yamagata et al. (1966), are shown in Supplementary Table 4. The estimated ground deposition of ^{137}Cs values until December 2005 ranged from 0.51 to 2.28 kBq m^{-2} as of October 1, 2008 ($n = 22$, Supplementary Table 4).

The estimated ground deposition of ^{137}Cs in paddy topsoil until December 2005, based on Komamura et al. (1999), ranged from 0.79 to 7.47 kBq m^{-2} as of October 1, 2008 ($n = 14$, Supplementary Table 8).

The range of ^{137}Cs-GFO over Japan until January 1, 1970, was 0.64–4.37 kBq m^{-2} as of October 1, 2008 (revised from Aoyama et al., 2006). The estimated ^{137}Cs-GFO values until December 31, 2005, using a correction factor of 0.879 ranged from 0.73 to 4.97 kBq m^{-2}, of which the value of the Southern Ocean area ($<30°$ N) ranged from 0.73 to 1.94 kBq m^{-2}.

The range of the Observatory data (1.23–5.00 kBq m^{-2}) was approximately consistent with the ^{137}Cs-GFO range of Aoyama data (0.73–4.97 kBq m^{-2}). The range of Yamagata data was relatively low (0.51–2.28 kBq m^{-2}), which was lesser than the average of the Observatory data (2.47 kBq m^{-2}). The Komamura data covered a wider range (0.79–7.47 kBq m^{-2}), in which two plots recorded higher ^{137}Cs-GFO than the upper range of the Observatory data (Supplementary Table 8). The two plots were located in Joetsu city in Niigata Prefecture (7.47 kBq m^{-2}) and Nonoichi town in Ishikawa Prefecture (5.34 kBq m^{-2}). The values of the Observatory data for the nearest observatory from the two sampling plots in Komamura were 3.17 kBq m^{-2} for Niigata, located 120 km northeast from Joetsu, and 3.66 kBq m^{-2} for Kanazawa, located 9 km northeast from Nonoichi (Table 3).

3.4. Spatial distribution of ^{137}Cs-GFO of the Forest Inventory data

The nationwide variation in ^{137}Cs-GFO of the Forest Inventory was

Table 3

Proportionally estimated decay-corrected cumulative depositions of ^{137}Cs-GFO until December 2005 on local observatories implementing a short-term fallout assessment.

Observatory		^{137}Cs-GFO (kBq m^{-2})		% of observed ^{137}Cs-GFO to total estimated
Prefecture	City	Average	SD	
Japan Meteorological Agency				
Hokkaido	Wakkanai	3.45	0.78	3.0
Hokkaido	Kushiro	3.52	0.83	2.5
Ibaraki	Mito	2.48	0.20	8.4
Ibaraki	Tsukuba (MRI)	2.56	0.66	4.2
Ishikawa	Wajima	3.96	0.89	3.1
Tottori	Yonago	3.21	0.73	3.0
Okinawa	Naha	2.45	0.71	1.1
Okinawa	Ishigaki	1.86	0.49	1.5
Local authority				
Hokkaido	Sapporo	2.30	0.28	20.1
Aomori	Aomori	1.86	0.23	20.1
Miyagi	Sendai	3.05	0.37	20.1
Akita	Akita	3.92	0.48	20.1
Ibaraki	Mito	1.86	0.23	20.1
Saitama	Niiza	1.71	0.21	20.1
Tokyo	Shinjyuku	1.58	0.20	20.1
Kanagawa	Yokohama	1.69	0.21	20.1
Niigata	Niigata	3.17	0.39	20.1
Ishikawa	Kanazawa	3.66	0.45	20.1
Fukui	Fukui	4.76	0.58	20.1
Shizuoka	Shizuoka	1.79	0.22	20.1
Aichi	Nagoya	1.66	0.20	20.1
Kyoto	Kyoto	1.92	0.24	20.1
Osaka	Osaka	1.31	0.16	20.1
Hyogo	Kobe	1.37	0.17	20.1
Wakayama	Wakayama	1.23	0.15	20.1
Tottori	Tottori	3.33	0.41	20.1
Okayama	Okayama	1.25	0.15	20.1
Hiroshima	Hiroshima	1.50	0.18	20.1
Kochi	Kochi	2.47	0.30	20.1
Fukuoka	Fukuoka	1.77	0.22	20.1
Nagasaki	Nagasaki	2.25	0.28	20.1
Kagoshima	Kagoshima	1.77	0.22	20.1

Values are as of Oct. 1, 2008.

found, which was characterized by the high accumulation in the northeastern area along the Sea of Japan (Fig. 2a). The spatial distribution of the Observatory ^{137}Cs-GFO data showed a similar spatial pattern (Fig. 2b). The normal total annual precipitation displayed the spatial distribution of higher precipitation in the southwestern area along the Pacific Ocean, although the precipitation in the northeastern area along the Sea of Japan was relatively high (Fig. 2c). These trends were also shown by the least-squares means of ^{137}Cs-GFO of the Forest Inventory by region (Model 2.6.2), as shown in Supplementary Table 9.

3.5. Relation between ^{137}Cs-GFO and precipitation amount (model 2.6.1)

The Forest Inventory of ^{137}Cs-GFO on a plot basis was not linearly related to the total annual precipitation, although the correlation was significant (Fig. 3a, Supplementary Table 10). The area group was also significant for the Forest Inventory, in which the intercept for the Pacific Ocean side was smaller than that for the Sea of Japan side. The interaction of total annual precipitation and area group was also significant for the Forest Inventory, and the slope of the relation between the precipitation amount and ^{137}Cs-GFO was larger on the Sea of Japan side as compared to that on the Pacific Ocean side (Fig. 3a, Supplementary Table 10). This indicated that ^{137}Cs-GFO increased with the precipitation amount, while ^{137}Cs activity concentration in precipitation on the Sea of Japan side was higher than that on the Pacific Ocean side.

^{137}Cs-GFO did not significantly correlate with the total annual precipitation for the Observatory data and Yamagata data (Fig. 3b and c), while the relationship was significant for Komamura data (Fig. 3d). The

interaction of the total annual precipitation and area group was insignificant for the Observatory, Yamagata, and Komamura data. The statistical results of these model analyses are listed in Supplementary Table 10.

3.6. Difference in the ^{137}Cs-GFO of the Forest Inventory based on the forest site properties (model 2.6.2)

The least-squares means of ^{137}Cs-GFO of the Forest Inventory by forest site properties were determined for both cases normalized and non-normalized by the total annual precipitation (Supplementary Tables 5 and 6). The ^{137}Cs-GFO of the Forest Inventory was not significantly different across three major soil groups (i.e., brown forest soils, black soils, and immature soils) (Supplementary Table 5). Podzolic soils exhibited significantly lower ^{137}Cs-GFO than those of brown forest soils, black soils, immature soils, and red and yellow soils for cases normalized by the annual precipitation, although the number of podzol sites was very small ($n = 6$) (Supplementary Table 5). There was no significant difference in the ^{137}Cs-GFO of the Forest Inventory among the forest types (Supplementary Table 6).

3.7. Difference in the ^{137}Cs-GFO based on dataset category (model 2.6.3)

The total annual precipitation and climate-based region were significant explanatory variables for predicting ^{137}Cs-GFO (Table 4). Dataset category was an insignificant explanatory variable ($p = 0.3415$). Post hoc comparisons among dataset categories indicated no significant difference in ^{137}Cs-GFO between any pair of dataset categories, including the Forest Inventory and the Observatory (Fig. 4). The least-squares mean ($\pm$SE) of ^{137}Cs-GFO of the Forest Inventory, that is, the average ^{137}Cs-GFO adjusted for the effects of total annual precipitation and region, were 2.08 ± 0.09 kBq m^{-2}. This was 79.1% of the least-squares mean for that of the Observatory data (2.63 ± 0.34 kBq m^{-2}). The least-squares means of ^{137}Cs-GFO for Yamagata and Komamura were 1.47 ± 1.10 and 2.62 ± 0.34 kBq m^{-2}, respectively (Fig. 4).

For all the subsets of the Forest Inventory data divided by the sediment movement category, the total annual precipitation and climate-based region were significant explanatory variables for predicting the ^{137}Cs-GFO (data not shown). The dataset category was not a significant explanatory variable for any subset ($p > 0.05$). The least-squares means of ^{137}Cs-GFO are shown elsewhere (Supplementary Table 11).

3.8. Variation in the ^{137}Cs-GFO of the Forest Inventory within a NFSCI sampling plot (model 2.6.4)

Using the GLM analysis, the ratio of the variance components of the NFSCI sampling plot as a random effect to the error variance was determined to be 0.702, and as a portion of the total variance, the value was 41.22%. The variance component estimate within the NFSCI sampling plot variability (58.8%) was greater than the variability among the NFSCI sampling plots (41.2%).

3.9. Difference in the ^{137}Cs-GFO of the Forest Inventory based on the sediment movement category (model 2.6.4)

There was no significant difference in the ^{137}Cs-GFO of the Forest Inventory across the sediment movement categories ($F = 0.1473$, $p = 0.8630$). The least-squares mean ($\pm$SE) of the ^{137}Cs-GFO of the Forest Inventory for each category are shown elsewhere (Supplementary Table 7).

3.10. Difference in the ^{137}Cs-GFO of the Forest Inventory based on the vertical distribution pattern (model 2.6.3 and 2.6.4)

We found significant differences in the ^{137}Cs-GFO of the Forest Inventory among a total of 11 vertical distribution patterns (nine Types
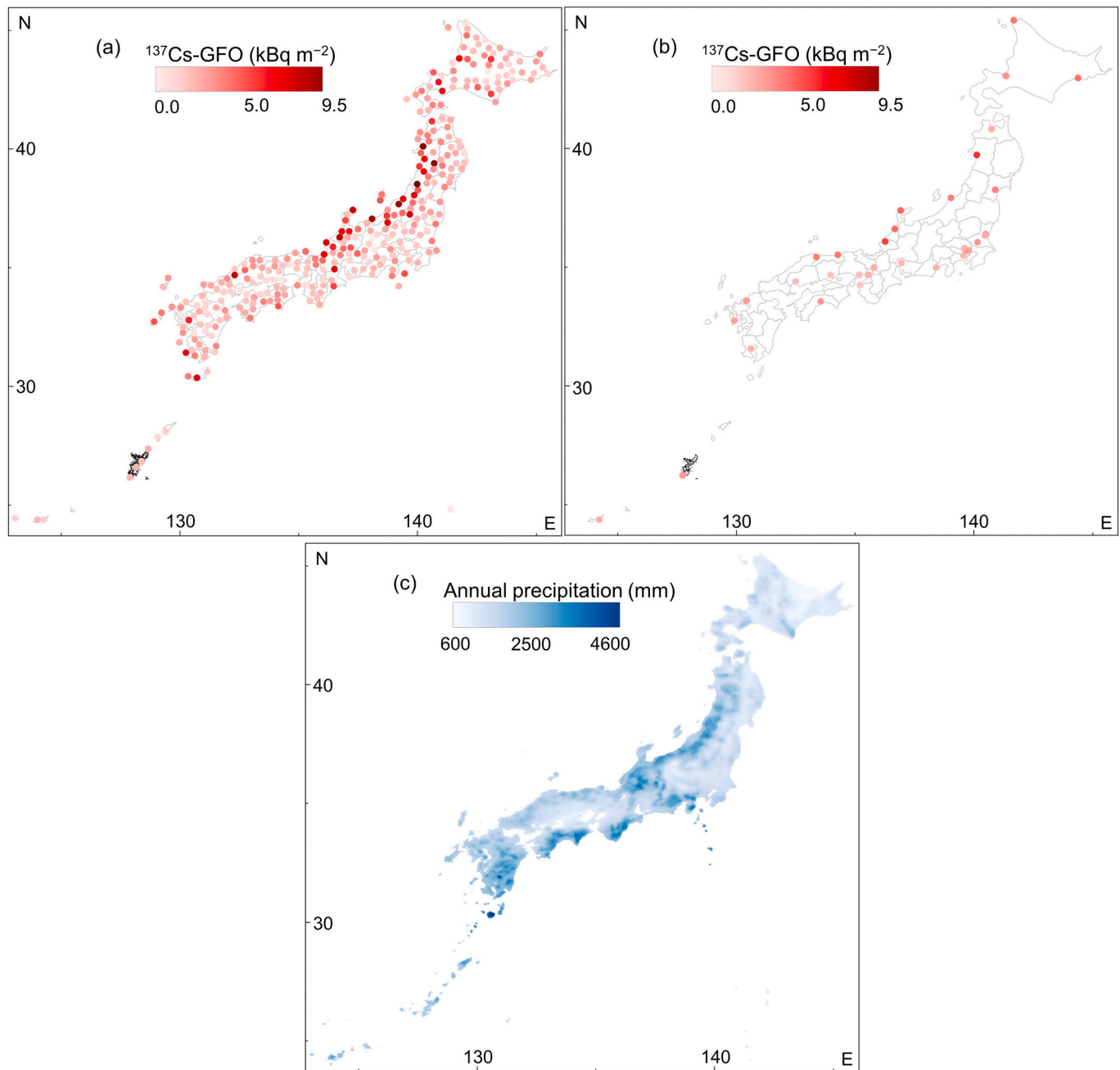
Fig. 2. Spatial distribution of ^{137}Cs-GFO and precipitation across Japan. (a) Forest Inventory data on a plot basis, (b) Observatory data, and (c) normal annual precipitation. The value of ^{137}Cs-GFO is shown as of Oct. 1, 2008.

and three Subtypes for Type 1) ($F = 17.10$, $p < 0.0001$, model 2.6.4). The least-squares mean ($\pm$SE) of ^{137}Cs-GFO of the Forest Inventory for each pattern and the results of the post hoc Tukey-HSD test are shown in Fig. 5. The patterns showing relatively low ^{137}Cs-GFO (Types 1–5) were common in that at least one layer contained a little amount of ^{137}Cs-GFO ($\exists n : Pn < 0.5$, Table 1). In particular, Type 2 (accumulation only in the first layer) displayed very low ^{137}Cs-GFO accumulation. The highest ^{137}Cs-GFO was found in Type 8, followed by Types 7 and 6 (Fig. 5).

A significant difference in the ^{137}Cs-GFO was found between the Observatory and the subset of the Forest Inventory extracting vertical distribution pattern of Types 1c, 2, 3, ($p < 0.0001$), 4 ($p = 0.011$) and 9 ($p = 0.075$), in which the Forest Inventory was significantly smaller than that of the Observatory (Table 1, model 2.6.3). On the other hand, there was no significant difference for the subset extracting Types 1a, 1b, 5, 6, 7, and 8 ($p > 0.05$) (Table 1). The least-squares mean of the Forest

Inventory was smaller than that of the Observatory for Types 1a, 1b, 5, and 6, while it was reversed for Types 7 and 8 (Table 1).

3.11. Combination of vertical distribution patterns coexisting in the same plot (model 2.6.5)

With respect to the vertical distribution patterns, which type coexists with a certain type within a plot was shown as a contingency table (Table 5). This contingency analysis was performed among nine Types of vertical distribution patterns. To ensure the number of samples in each cell of the contingency table, the three subtypes of Type 1 were analyzed together. The percentage of Type 2 accompanying Type 2 (14.2%) was higher than the total (overall) percentage of Type 2 appearance (6.3%). Similarly, Type 6 often coexisted with Type 6 (32.3%). The percentages of the same pattern appearing in the same plot were basically higher
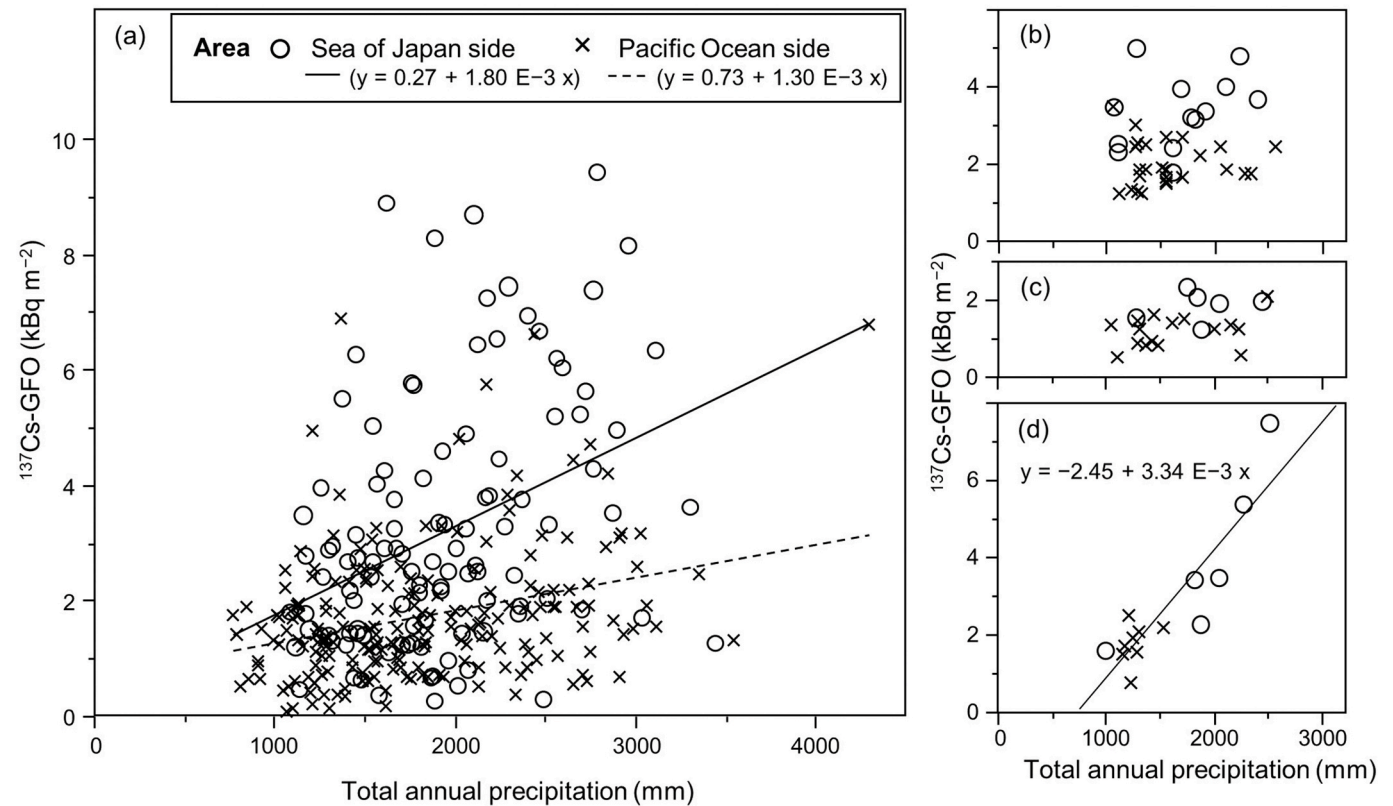
Fig. 3. Relations of ^{137}Cs-GFO against the total annual precipitation. (a) Forest Inventory data on a plot basis; (b) Observatory data; (c) Yamagata data; and (d) Komamura data. The value of ^{137}Cs-GFO is shown as of Oct. 1, 2008. White circles and X represent the area of the Sea of Japan side and Pacific Ocean side, respectively.

Table 4

Estimated variance components from the GLM model analysis for estimating ^{137}Cs-GFO.

Source	df	Denominator degrees of freedom	F-ratio	P
Precipitation	1	334.5	33.52	<.0001
Region	22	387.5	6.52	<.0001
Data category	3	382.4	1.12	0.3415
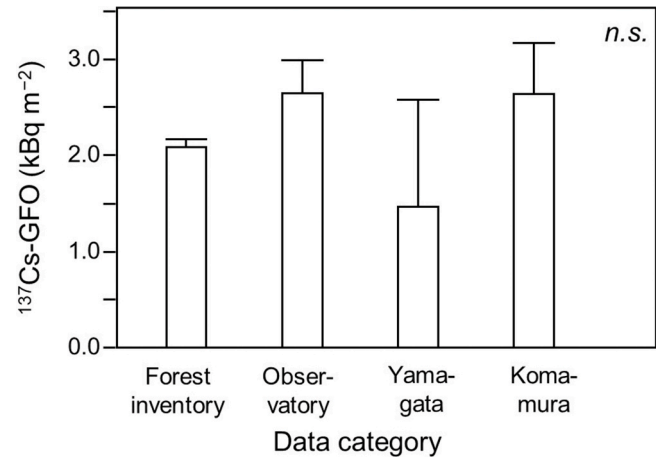
Fig. 4. Least-squares mean (±SE) ^{137}Cs-GFO across data categories. Post hoc comparisons between plot locations (Tukey-HSD test) are indicated by letters above the SE bars; statistics for the GLM model are given in Table 4.
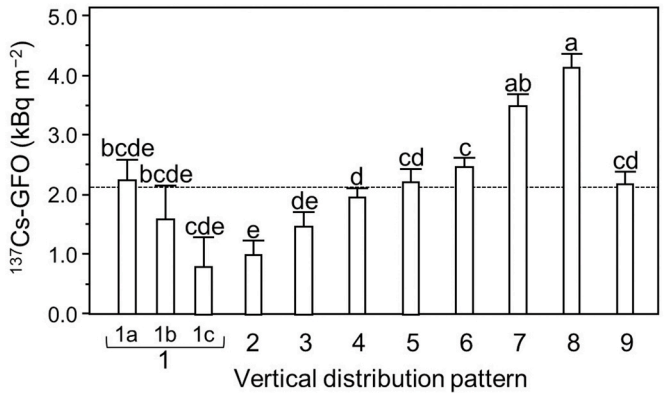
Fig. 5. Least-squares mean (±SE) ^{137}Cs-GFO across vertical distribution patterns. Post hoc comparisons between plot locations (Tukey-HSD test) are indicated by letters above the SE bars. Type 1 was subdivided into three Subtypes of 1a, 1b, and 1c. Horizontal dotted line indicates the overall average (2.14 kBq m^{-2}).

than the total percentage, except for Type 1 (Table 5). In determining the Chi-square values (shown as the lower values in parenthesis, Table 5), the highest Chi-square value was found for Type 2 accompanying Type 2 (19.6, bold font of lower values, Table 5), indicating that Type 2 tended to coexist with the same pattern in the same plot. A relatively high Chi-square value was found for Type 6 accompanying Type 6 (2.8).

The percentages of both Type 2 accompanying Type 3 (11.7%) and Type 3 accompanying Type 2 (12.3%) were higher than the total percentages (6.0% and 6.3%, respectively). High Chi-square values for this combination (10.7) indicated that Type 2 and Type 3 often appeared in

Table 5
Contingency table for the proportion of vertical distribution pattern appearing within the same NFSCI sampling plot for a given soil pit classified by the vertical distribution pattern.

Type	Vertical distribution pattern appearing in neighboring soil pits in the same plot								
	1	2	3	4	5	6	7	8	9
1	*3.2*	7.9	10.3	*23.8*	11.9	*20.6*	10.3	5.6	6.3
	(0.2)	(0.5)	**(4.0)**	(0.0)	**(7.0)**	**(3.2)**	(0.2)	(0.0)	(1.3)
2	5.1	14.2	11.7	*22.8*	*4.1*	25.4	*7.1*	*3.0*	6.6
	(0.5)	**(19.6)**	**(10.7)**	(0.1)	(1.3)	(1.0)	(0.8)	(2.7)	(1.8)
3	7.0	12.3	6.4	*20.9*	7.0	*24.6*	8.6	5.3	*8.0*
	(4.0)	**(10.7)**	(0.1)	(0.7)	(0.2)	(1.4)	(0.0)	(0.1)	(0.4)
4	*4.0*	*6.0*	*5.2*	24.6	*5.7*	29.4	9.1	6.0	9.9
	(0.0)	(0.1)	(0.7)	(0.1)	(0.1)	(0.0)	(0.0)	(0.0)	(0.1)
5	7.9	*4.2*	6.8	*22.6*	6.3	30.5	*7.9*	7.9	*5.8*
	(7.0)	(1.3)	(0.2)	(0.1)	(0.0)	(0.1)	(0.3)	(1.4)	(2.8)
6	*2.8*	*5.5*	*5.0*	24.0	6.3	32.3	*8.3*	5.2	10.5
	(3.2)	(1.0)	(1.4)	(0.0)	(0.1)	**(2.8)**	(0.5)	(0.6)	(0.9)
7	4.6	*5.0*	*5.7*	24.2	*5.3*	*27.0*	11.4	6.8	10.0
	(0.2)	(0.8)	(0.0)	(0.0)	(0.3)	(0.5)	(1.8)	(0.4)	(0.1)
8	*3.8*	*3.3*	5.5	24.6	8.2	*26.2*	10.4	8.7	*9.3*
	(0.0)	(2.7)	(0.1)	(0.0)	(1.4)	(0.6)	(0.4)	(2.6)	(0.0)
9	*2.7*	*4.4*	*5.0*	24.8	*3.7*	32.2	9.4	*5.7*	12.1
	(1.3)	(1.8)	(0.4)	(0.1)	(2.8)	(0.9)	(0.1)	(0.0)	(2.0)
Total	4.0	6.3	6.0	24.0	6.1	29.3	9.0	5.9	9.5

The type in the leftmost column indicates the vertical distribution pattern of a given soil pit. Upper values for each cell are percentages of each cell count to its row total. Add the upper values of each row to get 100 (%). The total percentage for each column shown in the bottom row is different from the appearance percentage of the total for each Type shown in Table 1, since this table represents pattern combination of a given soil pit and its neighboring pit. Italic font of upper values indicates that the value of each cell is lower than that of the total percentage for each column shown in the bottom row. Which type is more likely to appear for a given type can be suggested by comparing the upper value of each cell with the total percentage value. Lower values in parenthesis of each cell are Chi-square values. Higher Chi-square values indicate substantial deviations from the expected value for each cell. Bold font of lower values indicates the 10 highest Chi-square values. Note that there is no post hoc test to show statistical differences in values between each cell and expected in contingency table analysis.

the same plot. Similarly, Types 1–3 and 5 often appeared in the same plot.

Chi-square values for Type 4 were substantially small (≤ 0.77), which indicated that Type 4 was the least biased in terms of vertical distribution pattern for neighboring soil pits. In other words, it does not deviate from the expected value of the total percentages of appearance. Type 6 was also less biased; however, it often existed with Type 6 and was less accompanied by Type 1.

3.12. Simulation of the ^{137}Cs-GFO exports with sediment from the forested catchments (model 2.6.6)

The relationships of the accumulated sediment runoff percentage with the annual sediment runoff rate are shown in Supplementary Fig. 6. The least-squares mean of the ^{137}Cs-GFO of the Forest Inventory was 79.1% of that of the Observatory data (Section 3.6). Assuming that the missing 20.9% of the initial ^{137}Cs-GFO was due to the sediment runoff outside the forest catchment, the accumulated sediment runoff percentage of 20.9% as of October 1, 2008 requires a fixed sediment runoff rate of 0.522% year^{-1} if we alter the fixed rate (a white circle on the upper right side in Supplementary Fig. 6).

4. Discussion

4.1. Spatial distribution of the ^{137}Cs-GFO of the Forest Inventory: its relation to precipitation

To answer whether ^{137}Cs-GFO remains in forest soil across Japan, we prepared three datasets (Observatory, Yamagata, and Komamura data) as the initial values to compare ^{137}Cs-GFO of the Forest Inventory data. To properly compare data with different spatial densities, we incorporated the total annual precipitation into the GLM model as a fixed effect. Positive relations between ^{137}Cs-GFO and precipitation amount were found in the Forest Inventory (Fig. 3a) and Komamura data (Fig. 3d), as generally found both on land and over the ocean (Malakhov and Pudovkina, 1970; Aoyama and Hirose, 2003). The relation between the

Forest Inventory and total annual precipitation was not linear but rather ambiguous, where a range of slopes was detected in different areas (Fig. 3a). In other words, relatively high and low ^{137}Cs-GFO compared to the total annual precipitation was found along the Sea of Japan and in the southwestern part along the Pacific Ocean side, respectively (Fig. 2, Supplementary Tables 4 and 9).

To mitigate regional variation in the correlation between ^{137}Cs-GFO and precipitation amount, we introduced region category into the GLM model, thereby comparing the ^{137}Cs-GFO of the Forest Inventory with the other dataset categories under the normalized conditions of the total annual precipitation and region (Table 4). The high-^{137}Cs-GFO areas corresponded to the crossovers of areas with larger precipitation and a higher downward transport of radioactive aerosols from the stratosphere (Aoyama et al., 2006). Significant regional and/or seasonal variations in radioactive concentration in the rainfall have been reported in Japan (Malakhov and Pudovkina, 1970; Miyake et al., 1976; Katsuragi and Aoyama, 1986). While these studies suggest the need for aerologically appropriate regional classification, it is beyond the scope of this study. This study expediently used regional classification based on Yamagata et al. (1966), since Yamagata data only provided regional averages. The low correlation between fallout and precipitation amount is characteristic of Japan (Malakhov and Pudovkina, 1970). Further examinations are needed to ascertain which factors remarkably explain the high spatial variation in the amount of the initial ^{137}Cs-GFO across Japan.

4.2. Relevance of the ^{137}Cs-GFO of the Forest Inventory to site properties

The ^{137}Cs-GFO of the Forest Inventory was not related to the soil groups and forest types as stated in Section 3.6 (Supplementary Tables 5 and 6). The addition of these factors to the explanatory variables did not improve the prediction accuracy of the model for the ^{137}Cs-GFO of the Forest Inventory using the annual precipitation and region described in Section 4.1. Therefore, we did not consider these site properties in the following analysis.

4.3. Difference between the ^{137}Cs-GFO of the Forest Inventory and the observatory data

4.3.1. Results from the reference site approach

To assess the redistribution of ^{137}Cs fallout, the reference site approach has been well adopted (Walling and Quine, 1990; Wallbrink et al., 1994; Owens and Walling, 1996; Aoyama et al., 2006). The NFSCI soil samples, i.e., our Forest Inventory dataset samples, were collected at systematically selected locations (Supplementary Fig. 1, Ugawa et al., 2012, Section 2.1.1). The key limitation in adopting the reference site approach to the NFSCI dataset was whether the reference sites, i.e., undisturbed sites unaffected by soil erosion and accretion, could be appropriately extracted from the NFSCI dataset (Owens and Walling, 1996). Although there were concerns that the approach would be difficult to apply in this study, we attempted to classify the location of the soil pits based on microtopography and slope inclination into erosion, reference, and accumulation (see Section 2.5). There was no significant difference in the ^{137}Cs-GFO of the Forest Inventory among the sediment movement categories (Supplementary Table 7, see Section 3.9).

We compared the amount of ^{137}Cs-GFO between the Forest Inventory and the other dataset categories using the subset data classified by the sediment movement category (Supplementary Table 11). We expected (1) a significantly small ^{137}Cs-GFO of the Forest Inventory for the erosion subset, (2) no significant difference for the reference subset, and (3) a significantly large ^{137}Cs-GFO of the Forest Inventory for the accumulation subset. However, there was no significant difference for any subset (Supplementary Table 11, see also Section 3.7). These results did not change significantly even after adjusting the classification by microtopography or the slope inclination threshold (details are not shown). We determined that this conventional approach did not work in this study. This may be due to the difficulty of extracting appropriate reference sites from systematically located NF sampling points, as described above. We decline to proceed with any further discussion of the results obtained by applying this reference site approach.

4.3.2. Results from the GLM analysis normalized by the total annual precipitation and region

The GLM analysis indicated that the average ($\pm$SE) ^{137}Cs-GFO of the Forest Inventory adjusted for the effects of the total annual precipitation and region were 2.08 ± 0.09 kBq m^{-2} (Section 3.7). This value was slightly smaller than the average ($\pm$SE) non-adjusted ^{137}Cs-GFO (2.27 ± 0.10 kBq m^{-2}, Section 3.1.1). The former value (2.08 ± 0.09), adjusted for precipitation and regional effects by the GLM analysis, appears to be representative of the average ^{137}Cs-GFO of the Forest Inventory in Japan. A limitation of our GLM analysis is that the normalization based on the precipitation amount and regional classification is empirically determined as mentioned in the previous paragraph (see Section 4.1) but not theoretically established. Therefore, in this study, we avoid asserting that either is representative and instead only present the two values.

The GLM model analysis did not indicate a significant difference in ^{137}Cs-GFO between the Forest Inventory and the Observatory data (Fig. 4). The model also showed that the least-squares mean of ^{137}Cs-GFO of the Forest Inventory was 79.1% of that of the Observatory. This suggests that a substantial portion of ^{137}Cs-GFO (i.e., 79.1% of the total deposition) remained in the forest surface soil, while the rest (i.e., 20.9% of the total deposition) exists elsewhere other than in the surface soil. In addition to the limitations of the GLM described in the previous paragraph, the large uncertainties of the radiation activity measurements and the errors of more than half of the low activity concentration samples below the DL described in Section 3.1.1 cannot be ignored. Therefore, the numerical value indicating the degree of the remaining ^{137}Cs-GFO possibly includes errors due to unknown factors. In the following discussion, we consider the location of the missing portion of ^{137}Cs-GFO (approximately 20.9% of the total).

4.4. Possible locations of the missing ^{137}Cs-GFO

We consider the following three possible migration channels of the missing ^{137}Cs-GFO (i.e., ca. 20.9% of total deposition, see Section 4.3.2): (1) sediment discharge in stream water, (2) downward migration into the soil deeper than 30 cm, and (3) redistribution within the forest catchment.

4.4.1. Possibility of sediment discharge in stream water

The first possibility is sediment discharge in stream water, i.e., sediment runoff outside the forest catchment. It is of deep concern in steep, rainy terrains of Japan (Yamaguchi et al., 2012). We simulated the accumulated sediment runoff percentage given a fixed annual runoff rate over 60 years (Model 2.6.6), in which the accumulated runoff percentage of 20.9% was equivalent to the annual runoff rate of 0.52% year^{-1} (Supplementary Fig. 6). The reported annual runoff of ^{137}Cs of the total deposition of the catchment after the FDNPP accident ranged 0.3–0.5% year^{-1} in 2011 (Ueda et al., 2013), 0.019–0.3% year^{-1} in 2012–2013 (Iwagami et al., 2017), and 0.072% year^{-1} in 2014–2015 (Tsuji et al., 2016). The reported runoff rates are presumably too low to result in 20.9% of the initial ^{137}Cs-GFO loss in a duration longer than several years for the FDNPP accident case. Of course, we must recognize the uncertainty of the 20.9% figure (see Section 4.3). The annual runoff rate of 0.3% year^{-1}, for example, was equivalent to 12.6% of the accumulated discharge percentage over 50 years (Supplementary Fig. 6).

However, it should be noted that there are aspects of both overestimation and underestimation in the estimates applied throughout Japan from the Fukushima study, as described below. First, the measurements based on the runoff rate immediately after the accident are potentially overestimated, because the annual ^{137}Cs runoff rate decreases exponentially over time (Kato et al., 2017). Secondly, considering geological factors, the measurements might be underestimated. The Pacific coast region of Fukushima Prefecture is an area with a low landslide density, like the eastern Pacific coast of Hokkaido and the Ryukyu Islands (Saito et al., 2014, see also Section 4.4.3). Furthermore, there is the possibility of underestimation in terms of climate factors. The total annual precipitation in the study area of Fukushima (ca. 1100–1500 mm) is within the 25%–50% range of distribution in Japan (Japan Meteorological Agency, 2012). Sediment runoff rates may be higher in heavy rainfall areas. However, the effect of the precipitation amount could be negligible based on reports that only 0.07% of the total deposition of the catchment was discharged during a typhoon flood event in Fukushima (Shinomiya et al., 2014), and that the loss of ^{137}Cs-GFO associated with eroded sediment was estimated as 0.013% year^{-1} after decades from the catchment with high precipitation (>2000 mm year^{-1}) (Fukuyama et al., 2005).

Furthermore, we must consider the impact of the uncertainty (mentioned in Section 4.3.2) of the estimated percentage of the missing ^{137}Cs-GFO (i.e., 20.9% total deposition) on the conclusions. If the value of 20.9% was underestimated, the difference in the ^{137}Cs-GFO between the Forest Inventory and the Observatory would be greater, and this difference might be significant. However, such a high percentage of the missing ^{137}Cs-GFO is unexplained by the relatively low sediment runoff rates observed at Fukushima. This does not change the conclusion that the losses from sediment runoff were not a major factor in the redistribution of ^{137}Cs-GFO. Conversely, if the value of 20.9% was overestimated, then the relative importance of the sediment runoff process in the missing ^{137}Cs-GFO would be increased, and the differences in ^{137}Cs-GFO between the Forest Inventory and the Observatory data would be extremely small. This indicates that almost all of the ^{137}Cs-GFO depositions remain in the forest soils. This also does not change the conclusion described above.

4.4.2. *Possibility of downward migration into the soil to a depth of over 30 cm*

The second possibility is downward migration. The vertical infiltration of radionuclides has been the center of research interest for determining the environmental radionuclide-contamination on the global fallout, the Chernobyl-derived radionuclides (e.g., Bunzl et al., 1992; Barišić et al., 1999; Almgren and Isaksson, 2006; Shand et al., 2013), and on the FDNPP accident (Kato et al., 2012; Fujii et al., 2014; Nakanishi et al., 2014; Takahashi et al., 2015). Recent comprehensive meta-analysis study estimated that the ^{137}Cs-GFO penetration velocities ranged from 0.05 to 0.76 cm year^{-1} (median of 0.28 cm year^{-1}) over a 25-year period (Jagercikova et al., 2015).

However, we established that it was not the main cause of the missing ^{137}Cs-GFO with the following reasons based on the vertical distribution pattern (Table 1). Given no erosional and/or biological ^{137}Cs-GFO translocation, the difference in the vertical distribution pattern resulted from the variation in clay translocation velocity. We can assume that Type 2 remaining ^{137}Cs-GFO in the first layer corresponds to a very low infiltration rate, thereby allowing to take the expectation of high ^{137}Cs-GFO for Type 2. Meanwhile, we can assume that Type 8 having ^{137}Cs-GFO mainly in the second and third layers, rather than the first layer, corresponds to a very high infiltration rate, thereby allowing to take the expectation of low ^{137}Cs-GFO resulting from the infiltration ^{137}Cs loss into deeper soil. Completely contrary to these expectations, the lowest ^{137}Cs-GFO was found in Type 2, while the highest ^{137}Cs-GFO was found in Type 8 (Fig. 5).

These results suggest that downward migration is not the main cause of the missing ^{137}Cs-GFO. This is supported by the fact that most of the soil pits (Types 1c, 2, 4, 5, 6 and 7, 75.1% of the total) showed little or less ^{137}Cs-GFO accumulation in the third layer. This is also consistent with the results of low downward migration rates in mineral soil previously reported as 0.045 and 0.3 cm year^{-1} (Zygmunt et al., 1998), and 0.04, 0.15, and 0.45 in 0–2 cm, 2–5 cm, and 5–10 cm in depth, respectively (Bunzl et al., 1992). The reported migration rates are too low to result in infiltration to a depth of 30 cm over the past half a century, although more mobile ^{137}Cs-GFO was found in relatively deep soil layers decades after the deposition (Bunzl et al., 1998).

4.4.3. *Possibility of sediment redistribution within the forest catchment*

We propose that this third possibility of the transfer of slope materials downwards, i.e., a sediment redistribution within the forest catchment, is the most likely. The following three processes are assumed to be responsible for this sediment redistribution: landslides, soil creep, and soil erosion. These were similarly listed as processes of sediment delivery into headwater streams in a different study (Benda et al., 2005).

Landslide is defined internationally as "the movement of a mass of rock, earth, or debris down a slope" (Cruden, 1991); it was derived from mass movement (Penck, 1894). Landslides include various slope-movement processes under the influence of gravity: flow, slide, fall, and occasionally creep (Cruden and Varnes, 1996). The moving mass in landslides usually remains at or near the originating zone and is often displaced and disturbed (Varnes, 1978; Cruden and Varnes, 1996). The geological features in Japan resulted in an extremely high number of landslides globally (Yoshimatsu and Abe, 2006). Landslides occur repeatedly on even gentle to moderate slopes of 5–30° in Japan, where there are regional differences in frequency and type of movement due to geological factors (The Japan Society of Landslide and National Conference of Landslide Control, 2002). The return period of rainfall for rainfall-triggered landslides in Japan was estimated to be < 40 years for events including shallow landslides, debris flows, and rock slides (Saito et al., 2014), and <10^2–10^3 years for shallow landslides (Iida, 2004).

Soil creep is a low-velocity mass-movement phenomenon (Cruden and Varnes, 1996), in which slope materials deform slowly and move downward as a mass in the order of millimeters to centimeters annually. Soil creep was subdivided into seasonal soil creep and continuous (or mass rock, deep-sheeted) creep (Pawlik and Šamonil, 2018). The

seasonal soil creep is driven particularly by moisture and temperature fluctuations (e.g., frost heaving) and the activity of living organisms (Kirkby, 1967; Pawlik and Šamonil, 2018) The maximum soil creep rate is usually found at the top of the topsoil and occasionally at great depths (Clarke et al., 1999). Soil creep derived by moisture fluctuations has been monitored in Japan (Sasaki et al., 2000; Sonoda and Kurashige, 2017). Soil displacement of several mm per year acts as a prerequisite for future debris slides (Sasaki et al., 2000). Sonoda and Kurashige (2017) reported the phenomenon of miniature sliding in relation to soil creeping, where surface soil is displaced several mm or several cm when rainfall exceeds a certain threshold and shear deformation concentrates into a narrow zone.

Soil erosion by water, which constitutes almost all soil erosion in Japan, involves the processes of soil particle detachment, transport, and deposition on land surfaces (Renard and Foster, 1983). Before the peak of the ^{137}Cs-GFO deposition, sediment runoff rates from mountainous area to water channels were in the order of 10^{-2} to 10^{-1} mm year^{-1} in Japan; however, rates from bare land increased to the order of 10^0 mm year^{-1} (Kawaguchi, 1951). Since the rates are only for the sediment runoff to channels, the amount of soil displacement at a given point would be greater. Splash erosion is the primary agent for the detachment of soil particles (Dunne et al., 2010). On the land surfaces of densely forested or forest floor overgrazed by wild deers, prevalent in recent Japan, splash erosion is often the major contributor to soil erosion (Miyata et al., 2009; Ghahramani et al., 2011; Suzuki and Ito, 2014), although overland flow erosion and inter-rill erosion are the dominant transport mechanisms into stream channels (e.g., Gomi et al., 2008). The occurrence of erosion may be mitigated by forest floor coverage, which reduces the kinetic impact of raindrops (Durán and Rodríguez, 2008; Nanko et al., 2011; Miura et al., 2015b). Soil erosion is closely related to the distribution of ^{137}Cs in forests, and thus, ^{137}Cs has been used as a major tracer for many years (Ritchie and McHenry, 1990).

The third possibility, i.e., the sediment redistribution within the forest catchment, is attributed to the inevitably expected microscale heterogeneity of the ^{137}Cs-GFO distribution on the slope. The microscale heterogeneity of ^{137}Cs-GFO was suggested by the wider range and L-shape frequent distribution found on a soil pit basis rather than that on a plot basis (Fig. 1a and b). Moreover, the ^{137}Cs-GFO variability within the NFSCI sampling plots (58.8% of the total) was greater than that among the plots (i.e., 41.2%, see Section 3.8). This considerable variation among ~4 soil pit repetitions within a 0.1 ha plot strongly indicated the microscale heterogeneity of the ^{137}Cs-GFO distribution within a catchment. Such a spatially uneven radionuclide distribution has been reported in several forest ecosystems (Copplestone et al., 2000; Rawlins et al., 2002; Onda et al., 2015). Based on the results of the vertical distribution pattern analyses, we further examined this third possibility in the following section.

4.5. *Vertical distribution pattern explaining the cumulative slope-movement processes*

4.5.1. *Patterns suggesting erosion*

Considering the sediment migration within the catchment as the main cause of the vertical distribution pattern, the surface-concentrated Type 2 and Type 4 can be assumed to be subjected to fast and slow erosion, respectively. Type 4 is the second most frequent pattern (23.3% in total), found in 59% plots of the total (Table 1, see also Section 3.1.2), and least biased to accompanying patterns (Table 5, Section 3.11). Moreover, it was found that the relatively low ^{137}Cs-GFO for Type 2 and Type 4 (Fig. 5) and significantly lower ^{137}Cs-GFO of the subset of the Forest Inventory extracting soil pits of Types 2 and 4, as compared to the Observatory (Table 1). This does not prove that all the soil pits of Types 2 and 4 were subjected to fast erosion and slow erosion (or soil creep), respectively. The very slow infiltration rate of ^{137}Cs in soils may have resulted in this vertical distribution pattern, at least in some soil pits. These results, however, provide a general insight that a large part of the

forested area was subject to slow and mild erosion or soil displacement by soil creep. This insight conforms with the report that forestry environments were characterized by significant sediment redistribution (Croke et al., 1999; Croke and Nethery, 2006; Gomi et al., 2008).

4.5.2. Patterns suggesting stability

The most frequent pattern, Type 6, was 29.0% of the total soil pits, while it appeared in more than half (65.8%) of the NFSCI plots (Table 1, see also Section 3.1.2). In Type 6, ^{137}Cs-GFO gradually decreased with depth (Table 1). There was no significant difference in ^{137}Cs-GFO between the Forest Inventory of Type 6 and the Observatory (Table 1). Moreover, the smallest difference in the least-squares mean of ^{137}Cs-GFO was found between Type 6 subset of the Forest Inventory and the Observatory data among the nine Types (Table 1). These findings showed that ^{137}Cs-GFO remains in place where it is suggested that it has been stable with no erosion or redeposition over the past half a century.

4.5.3. Patterns suggesting redeposition

Type 8 (5.7% in total) and Type 7 (9.0% in total) showed the highest and second-highest ^{137}Cs-GFO accumulation (Fig. 5) whereby no significant but relatively larger ^{137}Cs-GFO inventory was found in the subset of the Forest Inventory rather than the Observatory (Table 1). In addition, both Type 8 and Type 7 were common in less ^{137}Cs-GFO per unit depth in the first layer than the second layer (i.e., $Q_1 < Q_2$) and in considerable ^{137}Cs-GFO accumulation in the third layer (Table 1). These results suggested that Type 8 and Type 7 resulted from the redeposition of eroded soil from the surrounding area.

One possible reason why ^{137}Cs-GFO was relatively low in the first layer for these Types could be the soil migration in successive years. The soil in the upper layer could be accumulated in recent years, which likely comprised a collection of soil from the surrounding area where the former surface soil containing considerable ^{137}Cs-GFO has already eroded. Another possible explanation was the disturbance of the masses, i.e., mixing of the topsoil and subsoil, accompanied by certain mass movements (Varnes, 1978). The considerably large Q_n values found in the second and third layers were comparable to those in the first layer (Supplementary Fig. 5, Section 3.1.1). This can be explained by the idea that former surface soils have accumulated over a small area due to secondary migration.

Given that considerable ^{137}Cs-GFO was found in the third layer for Type 8 and Type 7, it is more reasonable that ^{137}Cs-GFO exists even deeper than the third layer (>30 cm in depth) in such redeposited-oriented spots within a forest catchment. This could explain the question of why the ^{137}Cs-GFO of the Forest Inventory was relatively lower than that of the Observatory (see Section 4.3.2); this is because a part of ^{137}Cs-GFO was locally pooled in the deep soil.

These findings further indicate that ^{137}Cs-GFO remained in the forest after decades, as confirmed by Fukuyama et al. (2008), who showed that the losses and gains of fallout radionuclides balance at the landscape scale. The following observations can be drawn from this study on the distribution of ^{137}Cs-GFO in forest ecosystems after decades of deposition: ^{137}Cs-GFO was slightly less distributed on the surface soil in most areas of the forest and was locally concentrated in areas where it was stored in the deep soil.

4.5.4. Patterns suggesting multiple and complex occurrences of sediment redistribution

The importance of considering multiple spatial and temporal scales in geomorphic processes has been demonstrated (García-Ruiz et al., 2010). The other vertical distribution patterns (Types of 1, 3, 5, and 9) very likely suggested multiple and complex processes of ^{137}Cs-GFO redistribution on slopes. Types 1b and 3 had substantially thick soil layers (10 or 15 cm in depth) containing little ^{137}Cs-GFO (Table 1). Such ^{137}Cs-GFO-poor soil layers suggested the occurrence of landslides (i.e., mass movement), where considerable subsoil migrated to a different location. These two types were 7.0% of the total soil pits, which may

indicate the probability of occurrence of landslides during the past half century in Japan.

Types of 3, 5, and 9 might suggest multiple occurrences of sediment movements. Type 5 possibly suggests that small-scale erosion and redeposition were repeated for many years, where the surface soil was gradually replaced by the former subsoil from the surrounding area. Types 3 and 9 had the first layers containing more ^{137}Cs-GFO than the second layers (Table 1). This result suggests that secondary migration of ^{137}Cs-GFO on slopes has occurred multiple times during the last half century.

4.6. Coexisting vertical distribution patterns suggesting the scale of sediment movement events

The contingency analysis for coexisting vertical distribution patterns (Table 5, Section 3.11) indicated that Type 2 often coexisted with Types 2 and 3; Type 2 and Type 3 suggested fast erosion (Section 4.5.1) and considerable subsoil migration (Section 4.5.4), respectively; and that Type 6 suggesting stability often existed with Type 6 and was less accompanied by Type 1 suggesting sediment migration. This finding provided insights that soil pits with similar characteristics were often observed within the same NFSCI sampling plot with an area of 1000 m^2. This suggests that the spatial scale of soil disturbance was often approximately or more than 10^{-1} ha in forested areas in Japan.

4.7. Difficulties in determining the downward migration rate of ^{137}Cs in soils

The infiltration rate of ^{137}Cs in soils is the key factor in determining the fate of deposited ^{137}Cs on land, in which the Chernobyl-derived ^{137}Cs has been examined using dispersion–convection models or other models (Bunzl et al., 2000; Kirchner et al., 2009; Jagercikova et al., 2015). Studies on the downward migration of ^{137}Cs within 10 years after the FDNPP accident have indicated the low mobility of ^{137}Cs in surface mineral soils, where most of the ^{137}Cs were restricted to the upper 5 cm of the soil (Kato et al., 2012; Fujii et al., 2014; Nakanishi et al., 2014; Takahashi et al., 2015; Imamura et al., 2020). To clarify the long-term downward migration rates of ^{137}Cs in Japan, it is necessary to confirm that study sites had been undisturbed, i.e., unaffected by soil erosion and accretion, which is known as the reference site approach (as Yamagata et al. (1966) examined, see Section 2.3).

The conventional reference site approach, however, did not work well in predicting the residual amount of ^{137}Cs-GFO in this study (Sections 2.5 and 4.3.1). Instead, we utilized vertical distribution pattern-based analysis, which suggested the possibility of sediment redistribution (Section 4.5). It is theoretically difficult to estimate the downward migration rate using the subset extracting undisturbed soil pits based on the vertical distribution pattern, e.g. Type 6, which is the most stable pattern (Table 1). In this case, neglecting Type 7 leads to the underestimation of the rates. Type 7 is characterized by relatively low ^{137}Cs-GFO in the first layer, and it has the potential to be stable with relatively high downward migration rates. The stability of soils in the determination of the long-term infiltration rates of ^{137}Cs must be carefully assured based on land use history and site conditions, as described in Koarashi et al. (2017).

4.8. Forest management control of ^{137}Cs-GFO migration

This study provides insights into the ^{137}Cs-GFO migration and confirms previous findings on slope-movement processes (see Section 4.4.3). Moreover, we provide additional evidence on the soil erosion and mass movements of the forest floor in Japan over the past half century derived from the national representative dataset. These findings are summarized in Table 1, which shows the nine types of vertical distribution patterns and their frequency of appearance. The most frequent pattern, Type 6 (29.0% of the total soil pits, Section 4.5.2), suggested

that the forest floor surface is relatively stable, i.e., less sediment transfer over the past 50 years. The second frequent pattern, Type 4 (23.3% of the total soil pits, Section 4.5.1), suggested slow erosion. Both these types indicated moderate sediment migrations among the vertical distribution patterns. However, slope inclination, which is probably the dominant factors in soil erosion, was substantially large for both Type 6 and Type 4, averaging 25–26°, and was not significantly different from other Types (Table 1, Section 3.1.2). In addition, both Type 6 and Type 4 appeared in more than half of the NFSCI plots, 65.8% and 59.2%, respectively (Table 1, Section 3.1.2). Type 6 and Type 4 were ubiquitous; in other words, they appear everywhere in Japan. This suggests that the factors in soil erosion that are closely related to these Types were not the inherent properties of the land: such as slope inclination, slope length, or soil type (Miura et al., 2015a). A possible factor was the forest floor coverage. Miura et al. (2000; 2002; 2003; 2015b) clearly verified that the forest floor coverage governed the sediment transport by splash erosion in cypress plantation, where soil erosion problems are most prominent in Japanese forests. The forest floor coverage varies with the forest type, stand age, and forest management over months and years. If a site had not experienced significant mass movement, such as landslides, in the last 50 years, then the forest floor coverage may be a factor in determining the extent of sediment movement.

This study also indicated that considerable sediment movements frequently occurred in Japan since the 1950s. Pattern types other than Types 6 and 4, which suggested multiple and substantial erosion and consequent redeposition, accounted for 47.7% of the total soil pits (Table 1, Sections 4.5.1, 4.5.3, and 4.5.4). Erosion rates are definitely influenced by land use history (Miura et al., 2003; Wakiyama et al., 2010; Shinohara et al., 2019). Over-logging of forests induces soil erosion (García-Ruiz et al., 2017), and even if the logging pressure decreases, the effects will continue for about 20 years (Tada, 2018). In Japan, sediment-related disasters occurred frequently from 1950 to 1985 due to an increase in the extensive deforestation area during and after WWII (Tada, 2018). The periods of the global fallout coincided with the frequent occurrence of slope failures, which may have increased the secondary migration of fallouts after the initial deposition. In essence, the forest management history over the past half century may be closely related to the ^{137}Cs-GFO migration.

4.9. Biological and geological factors causing ^{137}Cs-GFO migration

Several factors that may affect the ^{137}Cs-GFO migration have not been addressed yet. The vertical distribution patterns cannot be simply explained by soil migration, e.g., Type 9 with the least ^{137}Cs-GFO amount in the second layer; a possible explanation is plant/fungi accumulation and translocation (Gillett and Crout, 2000; Sakashita et al., 2020). Moreover, resuspension and redeposition via fungal spore could induce annual spatial migration up to 0.1–0.3% of the total deposition (Igarashi et al., 2019; Aoyama et al., 2020). These aspects were beyond the scope of this study; however, future studies on the ^{137}Cs-GFO of the Forest Inventory should focus on bioturbation (Jarvis et al., 2010; Jagercikova et al., 2015).

Finally, we wish to discuss the effects of geology. Geological factors can affect the mobility of ^{137}Cs-GFO. Firstly, we discuss the geological factors related to the potential for landslides, a type of mass movement. Landslides frequently occur in large-scale faults and fracture zones, areas with tertiary sedimentary soft rocks, and volcanic zones in Japan (Yoshimatsu and Abe, 2006). Such areas are prone to slope movement of ^{137}Cs-GFO due to landslides. Secondarily, geological factors also affect the vertical distributions of ^{137}Cs in soils via the clay translocation velocity (Jagercikova et al., 2015). The landscape-scale variation in ^{137}Cs-GFO residuals might be well explained by the spatial estimates of the parent material, differing in quality and quantity of clay minerals, based on the ^{137}Cs adsorption potential (Kawase and Yokoyama, 1973; Rawlins et al., 2002; Nakao et al., 2012). The mineralogical properties and distribution of clay minerals with high ^{137}Cs adsorption potential

have been reported across Japan (The mining and metallurgical institute of Japan, 1984). Although this study is unable to encompass the entire geological factors, it is necessary to explicitly distinguish the effects of geological factors when discussing the variations in the horizontal and vertical migration of ^{137}Cs-GFO on the scale of the Japanese archipelago.

5. Conclusion

This study offers an exhaustive investigation of ^{137}Cs in the forest ecosystem before the FDNPP accident across Japan. This study provides insights for ensuring appropriate forest management planning. We examined the differences between the residual ^{137}Cs-GFO in forest soils (up to 30 cm depth) and the cumulative ^{137}Cs-GFO obtained from continuous fallout observation. The GLM model revealed that most of the deposited ^{137}Cs-GFO remained in the forest for more than half a century. The residual ^{137}Cs-GFO in the forest surface soil was not significant but relatively less than the cumulative ^{137}Cs-GFO, and considerable slope-scale spatial variation within the 0.1 ha plot was observed. Moreover, the vertical distribution pattern of ^{137}Cs-GFO in the soil profiles correlated with the amount of ^{137}Cs-GFO in forest soil. These findings provided a solid evidence base confirming that ^{137}Cs-GFO considerably underwent secondary migration on slopes within a forest catchment. In addition, some vertical distribution patterns suggested that ^{137}Cs-GFO can accumulate in deep soil layers (>30 cm in depth). This study also presented fundamental characteristics related to the amount of cumulative and residual ^{137}Cs-GFO in forest soils: left-biased frequency distribution, nationwide spatial variation that is greater in the northwestern part along the Sea of Japan, and significant but unclear relation to the precipitation amount.

Declaration of competing interest

The authors declare that they have no known competing financial interests or personal relationships that could have appeared to influence the work reported in this paper.

Appendix A. Supplementary data

Supplementary data to this article can be found online at https://doi.org/10.1016/j.jenvrad.2020.106421.

References

Almgren, S., Isaksson, M., 2006. Vertical migration studies of ^{137}Cs from nuclear weapons fallout and the Chernobyl accident. J. Environ. Radioact. 91, 90–102. https://doi.org/10.1016/j.jenvrad.2006.08.008.

Aoyama, M., 1999. Geochemical Studies on Behavior of Anthropogenic Radionuclides in the Atmosphere. Kanazawa University, Japan. PhD thesis.

Aoyama, M., Hirose, K., 2002. IGFD database – The Integrated Global Fallout Database, Version V40 as of 19 July 2002. https://www.mri-jma.go.jp/Dep/ap/ap4lab/recent/ge_report/dbhead.html.

Aoyama, M., 2019. The Integrated Global Fallout Database - IGFD. University of Tsukuba. https://doi.org/10.34355/CRiED.U.Tsukuba.00005.

Aoyama, M., Hirose, K., 2003. Temporal variation of ^{137}Cs water column inventory in the North Pacific since the 1960s. J. Environ. Radioact. 69, 107–117. https://doi.org/10.1016/S0265-931X(03)00089-4.

Aoyama, M., Hirose, K., Igarashi, Y., 2006. Re-construction and updating our understanding on the global weapons tests ^{137}Cs fallout. J. Environ. Monit. 8, 431–438. https://doi.org/10.1039/B512601K.

Aoyama, M., Tsumune, D., Inomata, Y., Tateda, Y., 2020. Mass balance and latest fluxes of radiocesium derived from the fukushima accident in the western North Pacific Ocean and coastal regions of Japan. J. Environ. Radioact. 217, 106206 https://doi.org/10.1016/j.jenvrad.2020.106206.

Arapis, G., Karandinos, M., 2004. Migration of 137Cs in the soil of sloping semi-natural ecosystems in Northern Greece. J. Environ. Radioact. 77, 133–142. https://doi.org/10.1016/j.jenvrad.2004.03.004.

Barišić, D., Vertačnik, A., Lulić, S., 1999. Caesium contamination and vertical distribution in undisturbed soils in Croatia. J. Environ. Radioact. 46, 361–374. https://doi.org/10.1016/S0265-931X(99)00011-9.

Benda, L., Hassan, M.A., Church, M., May, C.L., 2005. Geomorphology of steepland headwaters: the transition from hillslopes to channels. J. Am. Water Resour. Assoc. 41, 835–851. https://doi.org/10.1111/j.1752-1688.2005.tb03773.x.

Bunzl, K., Kracke, W., Schimmack, W., 1992. Vertical migration of plutonium-239+-240, americium-241 and caesium-137 fallout in a forest soil under spruce. Analyst 117, 469–474. https://doi.org/10.1039/AN9921700469.

Bunzl, K., Kracke, W., Schimmack, W., Zelles, L., 1998. Forms of fallout ^{137}Cs and $^{239+240}$Pu in successive horizons of a forest soil. J. Environ. Radioact. 39, 55–68. https://doi.org/10.1016/S0265-931X(97)00042-8.

Bunzl, K., Schimmack, W., Zelles, L., Albers, B., 2000. Spatial variability of the vertical migration of fallout ^{137}Cs in the soil of a pasture, and consequences for long-term predictions. Radiat. Environ. Biophys. 39, 197–205. https://doi.org/10.1007/s004110000062.

Clarke, M.F., Williams, M.A.J., Stokes, T., 1999. Soil creep: problems raised by a 23 year study in Australia. Earth Surf. Process. Landf. 24, 151–175. https://doi.org/10.1002/(SICI)1096-9837(199902)24:2<151::AID-ESP964>3.0.CO;2-G.

Copplestone, D., Johnson, M.S., Jones, S.R., 2000. Radionuclide behaviour and transport in a coniferous woodland ecosystem: the distribution of radionuclides in soil and leaf litter. Water Air Soil Pollut. 122, 389–404. https://doi.org/10.1023/A:1005225406105.

Croke, J., Nethery, M., 2006. Modelling runoff and soil erosion in logged forests: scope and application of some existing models. Catena 67, 35–49. https://doi.org/10.1016/j.catena.2006.01.006.

Croke, J., Hairsine, P., Fogarty, P., 1999. Runoff generation and re-distribution in logged eucalyptus forests, south-eastern Australia. J. Hydrol. 216, 56–77. https://doi.org/10.1016/S0022-1694(98)00288-1.

Cruden, D.M., 1991. A simple definition of a landslide. Bull. Int. Assoc. Eng. Geol.-Bulletin de l'Association Internationale de Géologie de l'Ingénieur 43, 27–29. https://doi.org/10.1007/BF02590167.

Cruden, D.M., Varnes, D.J., 1996. Landslide types and process. In: Turner, K.A., Schuster, R.L. (Eds.), Landslides: Investigation and Mitigation. Special Report 247, Transportation Research Board. National Research Council, U.S.A., pp. 36–75

Dunne, T., Malmon, D.V., Mudd, S.M., 2010. A rain splash transport equation assimilating field and laboratory measurements. J. Geophys. Res.: Earth Surf. 115, F01001 https://doi.org/10.1029/2009JF001302.

Durán, Z.V.H., Rodríguez, P.C.R., 2008. Soil-erosion and runoff prevention by plant covers. A review. Agron. Sustain. Dev. 28, 65–86. https://doi.org/10.1051/agro:2007062.

Dyer, A., Chow, J.K., Umar, I.M., 2000. The uptake of caesium and strontium radioisotopes onto clays. J. Mater. Chem. 10, 2734–2740. https://doi.org/10.1039/B006662L.

Evrard, O., Laceby, J.P., Lepage, H., Onda, Y., Cerdan, O., Ayrault, S., 2015. Radiocesium transfer from hillslopes to the Pacific Ocean after the Fukushima Nuclear Power Plant accident: a review. J. Environ. Radioact. 148, 92–110. https://doi.org/10.1016/j.jenvrad.2015.06.018.

Forest soils division, 1975. Classification of forest soil in Japan (1975). Bull. Gov. For. Exp. Stn. (Tokyo) 280, 1–28. https://www.ffpri.affrc.go.jp/labs/dfse/Profiles/img/SoilClassification1975.pdf.

Forestry Agency of Japan, 2012. Forest Resources Monitoring Survey in 1999–2008. https://www.rinya.maff.go.jp/j/keikaku/tayouseichousa/index.html.

Fujii, K., Ikeda, S., Akama, A., Komatsu, M., Takahashi, M., Kaneko, S., 2014. Vertical migration of radiocesium and clay mineral composition in five forest soils contaminated by the Fukushima nuclear accident. Soil Sci. Plant Nutr. 60, 751–764. https://doi.org/10.1080/00380768.2014.926781.

Fukuyama, T., Takenaka, C., Onda, Y., 2005. ^{137}Cs loss via soil erosion from a mountainous headwater catchment in central Japan. Sci. Total Environ. 350, 238–247. https://doi.org/10.1016/j.scitotenv.2005.01.046.

Fukuyama, T., Onda, Y., Takenaka, C., Walling, D.E., 2008. Investigating erosion rates within a Japanese cypress plantation using Cs-137 and Pb-210$_{ex}$ measurements. J. Geophys. Res. 113, F02007 https://doi.org/10.1029/2006JF000657.

García-Ruiz, J.M., Lana-Renault, N., Beguería, S., Lasanta, T., Regüés, D., Nadal-Romero, E., Serrano-Muela, P., López-Moreno, J.I., Alvera, B., Martí-Bono, C., Alatorre, L.C., 2010. From plot to regional scales: interactions of slope and catchment hydrological and geomorphic processes in the Spanish Pyrenees. Geomorphology 120, 248–257. https://doi.org/10.1016/j.geomorph.2010.03.038.

García-Ruiz, J.M., Beguería, S., Arnáez, J., Sanjuán, Y., Lana-Renault, N., Gómez-Villar, A., Álvarez-Martínez, J., Coba-Pérez, P., 2017. Deforestation induces shallow landsliding in the montane and subalpine belts of the Urbión Mountains, Iberian Range, Northern Spain. Geomorphology 296, 31–44. https://doi.org/10.1016/j.geomorph.2017.08.016.

Geochemical Research Department, 1996. Geochemical studies and analytical methods of anthropogenic radionuclides in fallout samples. Tech. Rep. Meteor. Res. Ins. 36 https://doi.org/10.11483/mritechrepo.36.

Ghahramani, A., Ishikawa, Y., Gomi, T., Shiraki, K., Miyata, S., 2011. Effect of ground cover on splash and sheetwash erosion over a steep forested hillslope: a plot-scale study. Catena 85, 34–47. https://doi.org/10.1016/j.catena.2010.11.005.

Gillett, A.G., Crout, N.M.J., 2000. A review of ^{137}Cs transfer to fungi and consequences for modelling environmental transfer. J. Environ. Radioact. 48, 95–121. https://doi.org/10.1016/S0265-931X(99)00060-0.

Gomi, T., Sidle, R.C., Miyata, S., Kosugi, K., Onda, Y., 2008. Dynamic runoff connectivity of overland flow on steep forested hillslopes: Scale effects and runoff transfer. Water Resour. Res. 44, W08411 https://doi.org/10.1029/2007WR005894.

Hashimoto, S., Ugawa, S., Nanko, K., Shichi, K., 2012. The total amounts of radioactively contaminated materials in forests in Fukushima,. Japan. Sci. Rep 2, 416. https://doi.org/10.1038/srep00416.

Igarashi, Y., Kita, K., Maki, T., Kinase, T., Hayashi, N., Hosaka, K., Adachi, K., Kajino, M., Ishizuka, M., Sekiyama, T.T., Zaizen, Y., Takenaka, C., Ninomiya, K., Okochi, H., Sorimachi, A., 2019. Fungal spore involvement in the resuspension of radiocaesium in summer. Sci. Rep. 9, 1954 https://doi.org/10.1038/s41598-018-37698-x.

Iida, T., 2004. Theoretical research on the relationship between return period of rainfall and shallow landslides. Hydrol. Process. 18, 739–756. https://doi.org/10.1002/hyp.1264.

Imamura, N., Matsuura, T., Akama, A., Ikeda, S., Kobayashi, M., Miura, S., Shinomiya, Y., Kaneko, S., 2020. Temporal changes in the spatial patterns of air dose rate from 2012 to 2016 at forest floors in Fukushima. Japan. J. Environ. Radioact. 222, 106377 https://doi.org/10.1016/j.jenvrad.2020.106377.

Iwagami, S., Onda, Y., Tsujimura, M., Abe, Y., 2017. Contribution of radioactive ^{137}Cs discharge by suspended sediment, coarse organic matter, and dissolved fraction from a headwater catchment in Fukushima after the Fukushima Dai-ichi Nuclear Power Plant accident. J. Environ. Radioact. 166, 466–474. https://doi.org/10.1016/j.jenvrad.2016.07.025.

Jagercikova, M., Cornu, S., Le Bas, C., Evrard, O., 2015. Vertical distributions of ^{137}Cs in soils: a meta-analysis. J. Soils Sediments 15, 81–95. https://doi.org/10.1007/s11368-014-0982-5.

Japan Meteorological Agency, 2007. Bulletin of the Radioactivity 89. ISSN 1349–2470.

Japan Meteorological Agency, 2012. Explanation of the Mesh Climatic Data of Japan 2010. Japan Meteorological Agency, Tokyo, p. 44.

Jarvis, N.J., Taylor, A., Larsbo, M., Etana, A., Rosén, K., 2010. Modelling the effects of bioturbation on the re-distribution of ^{137}Cs in an undisturbed grassland soil. Eur. J. Soil Sci. 61, 24–34. https://doi.org/10.1111/j.1365-2389.2009.01209.x.

Kato, H., Onda, Y., Teramage, M., 2012. Depth distribution of ^{137}Cs, ^{134}Cs, and ^{131}I in soil profile after fukushima Dai-ichi nuclear power plant accident. J. Environ. Radioact. 111, 59–64. https://doi.org/10.1016/j.jenvrad.2011.10.003.

Kato, H., Onda, Y., Hisadome, K., Loffredo, N., Kawamori, A., 2017. Temporal changes in radiocesium deposition in various forest stands following the Fukushima Dai-ichi Nuclear Power Plant accident. J. Environ. Radioact. 166, 449–457. https://doi.org/10.1016/j.jenvrad.2015.04.016.

Katsuragi, Y., 1983. A study of ^{90}Sr fallout in Japan. Pap. Meteorol. Geophys. 33, 277–291. https://doi.org/10.2467/mripapers.33.277.

Katsuragi, Y., Aoyama, M., 1986. Seasonal variation of Sr-90 fallout in Japan through the end of 1983. Pap. Meteorol. Geophys. 37, 15–36. https://doi.org/10.2467/mripapers.37.15.

Kawaguchi, T., 1951. Studies of soil erosion on mountain area. (1) Statistical studies by the former data. Rep. Gov. Forest Exp. Sta. 61, 1–44 (in Japanese with English abstract).

Kawase, K., Yokoyama, E., 1973. Strontium-90 and Cesium-137 levels in soils of various types at Niigata-Prefecture, Japan. J. Radiat. Res. 14, 40–48. https://doi.org/10.1269/jrr.14.40.

Kirchner, G., Strebl, F., Bossew, P., Ehlken, S., Gerzabek, M.H., 2009. Vertical migration of radionuclides in undisturbed grassland soils. J. Environ. Radioact. 100, 716–720. https://doi.org/10.1016/j.jenvrad.2008.10.010.

Kirkby, M.J., 1967. Measurement and theory of soil creep. J. Geol. 75, 359–378. https://www.jstor.org/stable/30085000.

Koarashi, J., Atarashi-Andoh, M., Amano, H., Matsunaga, T., 2017. Vertical distributions of global fallout ^{137}Cs and ^{14}C in a Japanese forest soil profile and their implications for the fate and migration processes of Fukushima-derived ^{137}Cs. J. Radioanal. Nucl. Chem. 311, 473–481. https://doi.org/10.1007/s10967-016-4938-7.

Komamura, M., Tsumura, A., Kodaira, K., 1999. Residence half-time of ^{137}Cs in Japanese paddy top-soils. Radioisotopes 48, 635–644. https://doi.org/10.3769/radioisotopes.48.635 (in Japanese with English abstract).

Mabit, L., Meusburger, K., Fulajtar, E., Alewell, C., 2013. The usefulness of ^{137}Cs as a tracer for soil erosion assessment: a critical reply to Parsons and Foster (2011). Earth Sci. Rev. 127, 300–307. https://doi.org/10.1016/j.earscirev.2013.05.008.

Malakhov, S., Pudovkina, I., 1970. Strontium 90 fallout distribution at middle latitudes of the Northern and Southern Hemispheres and its relation to precipitation. J. Geophys. Res. 75, 3623–3628. https://doi.org/10.1029/JC075i018p03623.

Miura, S., 2000. Proposal for a new definition to evaluate the status of forest floor cover and floor cover percentage (FCP) from the viewpoint of the protection against raindrop splash. J. Jpn. For. Soc. 82, 132–140. https://doi.org/10.11519/jjfs1953.82.2_132 (in Japanese with English abstract).

Miura, S., Hirai, K., Yamada, T., 2002. Transport rates of surface materials on steep forested slopes induced by raindrop splash erosion. J. For. Res. 7, 201–211. https://doi.org/10.1007/BF02763133.

Miura, S., Ugawa, S., Yoshinaga, S., Yamada, T., Hirai, K., 2015. Floor cover percentage determines splash erosion in *Chamaecyparis obtusa* forests. Soil Sci. Soc. Am. J. 79, 1782–1791. https://doi.org/10.2136/sssaj2015.05.0171.

Miura, S., Yoshinaga, S., Yamada, T., 2003. Protective effect of floor cover against soil erosion on steep slopes forested with *Chamaecyparis obtusa* (hinoki) and other species. J. For. Res. 8, 27–35. https://doi.org/10.1007/s103100300003.

Miura, S., Aoyama, M., Ito, E., Shichi, K., Takata, D., Masaya, M., Sekiya, N., Kobayashi, N., Takano, N., Kaneko, S., 2015a. Towards prediction of redistribution of fallout radiocesium on forested area discharged from Fukushima Nuclear Power Plant. In: EGU General Assembly Conference Abstracts, 17. EGU2015–8989. https://meetingorganizer.copernicus.org/EGU2015/EGU2015-8989.pdf.

Miyake, Y., Kanazawa, T., Saruhashi, K., Katsuragi, Y., 1976. A meteorological study on the local changes in radioactive fallout. Pap. Meteorol. Geophys. 27, 89–98. https://www.jstage.jst.go.jp/article/mripapers1950/27/3/27_89/_pdf.

Miyata, S., Kosugi, K., Gomi, T., Mizuyama, T., 2009. Effects of forest floor coverage on overland flow and soil erosion on hillslopes in Japanese cypress plantation forests. Water Resour. Res. 45, W06402 https://doi.org/10.1029/2008WR007270.

Nakajima, T., Misawa, S., Morino, Y., Tsuruta, H., Goto, D., Uchida, J., Takemura, T., Ohara, T., Oura, Y., Ebihara, M., 2017. Model depiction of the atmospheric flows of radioactive cesium emitted from the Fukushima Daiichi Nuclear Power Station accident. Prog. Earth and Planet. Sci. 4, 2 https://doi.org/10.1186/s40645-017-0117-x.

Nakanishi, T., Matsunaga, T., Koarashi, J., Atarashi-Andoh, M., 2014. ^{137}Cs vertical migration in a deciduous forest soil following the Fukushima Dai-ichi Nuclear Power Plant accident. J. Environ. Radioact. 128, 9–14. https://doi.org/10.1016/j.jenvrad.2013.10.019.

Nakao, A., Funakawa, S., Takeda, A., Tsukada, H., Kosaki, T., 2012. The distribution coefficient for cesium in different clay fractions in soils developed from granite and Paleozoic shales in Japan. Soil Sci. Plant Nutr. 58, 397–403. https://doi.org/10.1080/00380768.2012.698595.

Nanko, K., Onda, Y., Ito, A., Moriwaki, H., 2011. Spatial variability of throughfall under a single tree: experimental study of rainfall amount, raindrops, and kinetic energy. Agric. For. Meteorol. 151, 1173–1182. https://doi.org/10.1016/j.agrformet.2011.04.006.

Nanko, K., Hashimoto, S., Miura, S., Ishizuka, S., Sakai, Y., Levia, D.F., Ugawa, S., Nishizono, T., Kitahara, F., Osone, Y., Kaneko, S., 2017. Assessment of soil group, site and climatic effects on soil organic carbon stocks of topsoil in Japanese forests. Eur. J. Soil Sci. 68, 547–558. https://doi.org/10.1111/ejss.12444.

Onda, Y., Kato, H., Hoshi, M., Takahashi, Y., Nguyen, M.L., 2015. Soil sampling and analytical strategies for mapping fallout in nuclear emergencies based on the Fukushima Dai-ichi Nuclear Power Plant accident. J. Environ. Radioact. 139, 300–307. https://doi.org/10.1016/j.jenvrad.2014.06.002.

Owens, P.N., Walling, D.E., 1996. Spatial variability of caesium-137 inventories at reference sites: an example from two contrasting sites in England and Zimbabwe. Appl. Radiat. Isot. 47, 699–707. https://doi.org/10.1016/0969-8043(96)00015-2.

Parsons, A.J., Foster, I.D.L., 2011. What can we learn about soil erosion from the use of ^{137}Cs? Earth Sci. Rev. 108, 101–113. https://doi.org/10.1016/j.earscirev.2011.06.004.

Pawlik, Ł., Šamonil, P., 2018. Soil creep: the driving factors, evidence and significance for biogeomorphic and pedogenic domains and systems – a critical literature review. Earth Sci. Rev. 178, 257–278. https://doi.org/10.1016/j.earscirev.2018.01.008.

Penck, A., 1894. Morphologie der Erdoberfläche. Engelhorn, Stuttgart, 2 volumes.

Rafferty, B., Brennan, M., Dawson, D., Dowding, D., 2000. Mechanisms of ^{137}Cs migration in coniferous forest soils. J. Environ. Radioact. 48, 131–143. https://doi.org/10.1016/S0265-931X(99)00027-2.

Rawlins, B.G., Scheib, C., Beamish, D., Webster, R., Tyler, A.N., Young, M.E., 2002. Landscape-scale controls on the spatial distribution of caesium 137: a study based on an airborne geophysical survey across Northern Ireland. Earth Surf. Process. Landf. 36, 158–169. https://doi.org/10.1002/esp.2026.

Renard, K.G., Foster, G.R., 1983. Soil conservation: principles of erosion by water. Dryland Agric. 23, 155–176.

Ritchie, J.C., McHenry, J.R., 1990. Application of radioactive fallout cesium-137 for measuring soil erosion and sediment accumulation rates and patterns: a review. J. Environ. Qual. 19, 215–233. https://doi.org/10.2134/jeq1990.00472425001900020006x.

Rosén, K., Öborn, I., Lönsjö, H., 1999. Migration of radiocaesium in Swedish soil profiles after the Chernobyl accident, 1987–1995. J. Environ. Radioact. 46, 45–66. https://doi.org/10.1016/S0265-931X(99)00040-5.

Saito, H., Korup, O., Uchida, T., Hayashi, S., Oguchi, T., 2014. Rainfall conditions, typhoon frequency, and contemporary landslide erosion in Japan. Geology 42, 999–1002. https://doi.org/10.1130/G35680.1.

Sakashita, W., Miura, S., Akama, A., Ohashi, S., Ikeda, S., Saitoh, T., Komatsu, M., Shinomiya, Y., Kaneko, S., 2020. Assessment of vertical radiocesium transfer in soil via roots. J. Environ. Radioact. 222, 106369 https://doi.org/10.1016/j.jenvrad.2020.106369.

Sasaki, Y., Fujii, A., Asai, K., 2000. Soil creep process and its role in debris slide generation—field measurements on the north side of Tsukuba Mountain in Japan. Eng. Geol. 56, 163–183. https://doi.org/10.1016/S0013-7952(99)00141-6.

Schwarz, G., 1978. Estimating the dimension of a model. Ann. Stat. 6, 461–464. https://www.jstor.org/stable/2958889.

Shand, C.A., Rosén, K., Thored, K., Wendler, R., Hillier, S., 2013. Downward migration of radiocaesium in organic soils across a transect in Scotland. J. Environ. Radioact. 115, 124–133. https://doi.org/10.1016/j.jenvrad.2012.08.003.

Shinohara, Y., Misumi, Y., Kubota, T., Nanko, K., 2019. Characteristics of soil erosion in a moso-bamboo forest of western Japan: comparison with a broadleaved forest and a coniferous forest. Catena 172, 451–460. https://doi.org/10.1016/j.catena.2018.09.011.

Shinomiya, Y., Tamai, K., Kobayashi, M., Ohnuki, Y., Shimizu, T., Iida, S., Nobuhiro, T., Sawano, S., Tsuboyama, Y., Hiruta, T., 2014. Radioactive cesium discharge in stream water from a small watershed in forested headwaters during a typhoon flood event. Soil Sci. Plant Nutr. 60, 765–771. https://doi.org/10.1080/00380768.2014.949852.

Sonoda, M., Kurashige, Y., 2017. Characteristics of surface soil creep on a forest slope in Japan. Geomorphology 288, 1–11. https://doi.org/10.1016/j.geomorph.2017.03.006.

Suzuki, M., Ito, E., 2014. Combined effects of gap creation and deer exclusion on restoration of belowground systems of secondary woodlands: a field experiment in warm-temperate monsoon Asia. For. Ecol. Manag. 329, 227–236. https://doi.org/10.1016/j.foreco.2014.06.028.

Tada, Y., 2018. Landscape changes and disasters in Japan. Water science 62, 121–137. https://doi.org/10.20820/suirikagaku.62.4_121 (in Japanese, tentative translation).

Takahashi, J., Tamura, K., Suda, T., Matsumura, R., Onda, Y., 2015. Vertical distribution and temporal changes of ^{137}Cs in soil profiles under various land uses after the Fukushima Dai-ichi Nuclear Power Plant accident. J. Environ. Radioact. 139, 351–361. https://doi.org/10.1016/j.jenvrad.2014.07.004.

The Japan Society of Landslide and National Conference of Landslide Control, 2002. Landslides in Japan the sixth revision. https://japan.landslide-soc.org/wp19/wp-content/uploads/2019/05/2002.pdf.

The mining and metallurgical institute of Japan, 1984. Investigation on mineral resources for buffer materials. Japan nuclear cycle development institute, Ibaraki, Japan (In Japanese with English abstract). https://jopss.jaea.go.jp/pdfdata/PNC-TJ199-84-49VOL2.pdf.

Tsuji, H., Nishikiori, T., Yasutaka, T., Watanabe, M., Ito, S., Hayashi, S., 2016. Behavior of dissolved radiocesium in river water in a forested watershed in Fukushima Prefecture. J. Geophys. Res.: Biogeosciences 121, 2588–2599. https://doi.org/10.1002/2016JG003428.

Ueda, S., Hasegawa, H., Kakiuchi, H., Akata, N., Ohtsuka, Y., Hisamatsu, S., 2013. Fluvial discharges of radiocaesium from watersheds contaminated by the Fukushima Dai-ichi Nuclear Power Plant accident, Japan. J. Environ. Radioact. 118, 96–104. https://doi.org/10.1016/j.jenvrad.2012.11.009.

Ugawa, S., Takahashi, M., Morisada, K., Takeuchi, M., Matsuura, Y., Yoshinaga, S., Araki, M., Tanaka, N., Ikeda, S., Miura, S., 2012. Carbon stocks of dead wood, litter, and soil in the forest sector of Japan: general description of the National Forest Soil Carbon Inventory. Bull. For. For. Prod. Res. Inst. 425, 207–221. https://www.ffpri.affrc.go.jp/pubs/bulletin/425/documents/425-2.pdf.

Varnes, D.J., 1978. Slope movement types and processes. In: Schuster, R.L., Krizek, R.J. (Eds.), Landslides: Analysis and Control. Special Report 176, Transportation Research Board. National Research Council, U.S.A., pp. 11–33

Wakiyama, Y., Onda, Y., Mizugaki, S., Asai, H., Hiramatsu, S., 2010. Soil erosion rates on forested mountain hillslopes estimated using ^{137}Cs and ^{210}Pb$_{ex}$. Geoderma 159, 39–52. https://doi.org/10.1016/j.geoderma.2010.06.012.

Wallbrink, P.J., Olley, J.M., Murray, A.S., 1994. Variability in stream erosion and sediment transport. Proc. Canberra Symp., December 1994. IAHS Publ. 224, 95–102.

Walling, D.E., Quine, T.A., 1990. Calibration of caesium-137 measurements to provide quantitative erosion rate data. Land Degrad. Rehabilitation 2, 161–175. https://doi.org/10.1002/ldr.3400020302.

Yamada, T., Takano, N., 2014. Doublet peak area determination in NaI(Tl) scintillation spectrometry using maximum likelihood estimation. Appl. Radiat. Isot. 87, 407–409. https://doi.org/10.1016/j.apradiso.2013.11.069.

Yamagata, N., Iwashima, K., Matsuda, S., Tajima, E., 1966. Cumulative ground deposit of Cesium-137 in Japan. Bull. Inst. Publ. Health 15, 119 (in Japanese with English abstract).

Yamaguchi, N., Takata, Y., Hayashi, K., Ishikawa, S., Kuramata, M., Eguchi, S., Yoshikawa, S., Sakaguchi, A., Asada, K., Wagai, R., 2012. Behavior of radiocaesium in soil-plant systems and its controlling factor. Bull. Natl. Inst. Agro-Environ. Sci. 31, 75–129 (in Japanese with English abstract). http://dl.ndl.go.jp/info:ndljp/pid/11097079.

Yoshimatsu, H., Abe, S., 2006. A review of landslide hazards in Japan and assessment of their susceptibility using an analytical hierarchic process (AHP) method. Landslides 3, 149–158. https://doi.org/10.1007/s10346-005-0031-y.

Zhiyanski, M., Bech, J., Sokolovska, M., Lucot, E., Bech, J., Badot, P.-M., 2008. Cs-137 distribution in forest floor and surface soil layers from two mountainous regions in Bulgaria. J. Geochem. Explor. 96, 256–266. https://doi.org/10.1016/j.gexplo.2007.04.010.

Zygmunt, J., Chibowski, S., Klimowicz, Z., 1998. The effect of sorption properties of soil minerals on the vertical migration rate of cesium in soil. J. Radioanal. Nucl. Chem. 231, 57–62. https://doi.org/10.1007/BF02388005.